PASSIVE GLASS WAVEGUIDES FOR INTEGRATED OPTICS

By

RAJENDRA K. LAGU

A DISSERTATION PRESENTED TO THE GRADUATE SCHOOL
OF THE UNIVERSITY OF FLORIDA
IN PARTIAL FULFILLMENT OF THE REQUIREMENTS
FOR THE DEGREE OF DOCTOR OF PHILOSOPHY

UNIVERSITY OF FLORIDA

1985

ACKNOWLEDGMENTS

I would like to express my gratitude to my advisor Dr. V. Ramaswamy for his guidance and constant encouragement. I am indebted to my colleagues Paul Suchoski, Andrew Ardeman, Hanggeun Jeong and Iraj Najafi for their helpful suggestions and discussions during the course of this work. I would like to thank C. Wayne Twiddy for his help in waveguide polishing and E. J. Jenkins for his help in the SEM analysis. I would also like to express my gratitude to Ms. Betsy Childers and Carole Boone for their long hours of hard work and infinite patience in helping prepare this manuscript.

Last and certainly not the least, I shall always remain grateful to my parents and my wife for all that they have done to support me in all my endeavors.

TABLE OF CONTENTS

PAGE

ACKNOWLEDGMENTS....................................ii

LIST OF FIGURES....................................v

ABSTRACT...viii

CHAPTER

ONE INTRODUCTION....................................1

- 1.1 Optical Communication Systems....................1
- 1.2 Optical Computing................................4
- 1.3 Review of the Progress in Integrated Optics......5
- 1.4 Project Definition...............................10

TWO PROPAGATION ANALYSIS..............................18

- 2.1 Planar Step Index Waveguides.....................19
- 2.2 Planar Asymmetrical Graded Index Waveguides......24
- 2.3 Planar Graded Index Buried Waveguides............34
- 2.4 Graded Index Channel Waveguides..................37

THREE DIFFUSION SIMULATION............................74

- 3.1 One-Dimensional Diffusion without Drift Field....78
- 3.2 One-Dimensional Diffusion with Drift Field.......80
- 3.3 Two-Dimensional Diffusion with and without Drift Field....85

FOUR WAVEGUIDE FABRICATION............................102

- 4.1 Fabrication Process..............................102
- 4.2 Concentration Measurement........................106
- 4.3 Planar Waveguide Fabrication Procedure...........111

FIVE PLANAR WAVEGUIDE CHARACTERIZATION..........121

5.1 Mode Index Measurement..................121
5.2 Propagation Loss Measurement..............124
5.3 Index Profile Measurement 127

SIX PLANAR WAVEGUIDE DESIGN PROCEDURE..........142

6.1 Relations Between the Process and the Device Parameters...........................142
6.2 Design Procedure........................148

SEVEN SCOPE FOR FUTURE WORK.......................158

7.1 Mode Profile Measurement................158
7.2 Buried Waveguide Fabrication.............160
7.3 Channel Waveguide Fabrication.............161
7.4 Future Applications.....................162

EIGHT CONCLUSIONS..................................171

REFERENCES...173

BIOGRAPHICAL SKETCH...................................179

LIST OF FIGURES

FIGURE PAGE

1.1 An optical communication system....................14
1.2 Wavelength division multiplexing...................15
1.3 Transmitting end subsystem.........................16
1.4 Receiving end subsystem............................17

2.1 Ray diagram for the step index waveguide...........52
2.2 b-V characteristics for the step index waveguide.53
2.3 Ray diagram for the graded index waveguide.........54
2.4 Normalized index profile functions.................55
2.5 b-V characteristic for $m=0$ for various index profiles..........56
2.6 b-V characteristic for $m=0,1,2$ for Gaussian profile............57
2.7 Field profiles for $m=0$, $V=5,10,15$ for Gaussian profile..........58
2.8 Field profiles for $m=0,1,2$ for Gaussian profile..59
2.9 b-v characteristics for $m=0,1,2$ for erfc profile.60
2.10 Field profiles for $m=0$, $V=5,10,15$ for erfc profile..........61
2.11 Field profiles for $m=0,1,2$ for erfc profile......62
2.12 Effective normalized model width for $m=0$ for Gaussian profile..........63
2.13 Effective normalized modal width for $m=0$ for erfc profile..........64
2.14 Comparison of the field profile for $m=0$ for various index profiles..........65
2.15 Ray diagram for the buried waveguide...............66
2.16 b-V characteristics for the buried waveguide.......67
2.17 Channel waveguide geometry.........................68
2.18 Rectangular grid for the Variational-Finite difference method..........69
2.19 b-V characteristics for the step index channel waveguide with $r=1$..........70
2.20 b-V characteristics for the step index channel waveguide with $r=2$..........71
2.21 b-v characteristics, $m=0$, $r=1$, for channel waveguides with various index profiles..........72
2.22 b-V characteristics, $m=0$,$r=2$, for channel waveguides with various index profiles..........73

3.1 Rectangular grid for one dimensional diffusion simulation 89
3.2 Concentration profiles for one dimensional diffusion without applied field 90
3.3 Concentration profiles for field assisted diffusion for various diffusion times 91
3.4 Concentration profiles for field assisted diffusion for various values of the applied field 92
3.5 Tailoring of the index profile by an applied electric field 93
3.6 Concentration contours for E=0 V/mm, t=50 min., w=10 microns 94
3.7 Concentration contours for E=0 V/mm, t=50 min., w=5 microns 95
3.8 Concentration contours for E=30 V/mm, t=50 min., w=10 microns 96
3.9 Concentration contours for E=30 V/mm, t=50 min., w=5 microns 97
3.10 Concentration surface for E=0 V/mm, t=50 min., w=5 microns 98
3.11 Concentration surface for E=30 V/mm, t=50 min., w=5 microns 99
3.12 Concentration surface for E=0 V/mm, t=50 min., w=10 microns 100
3.13 Concentration surface for E=30 V/mm, t=50 min., w=10 microns 101

4.1 Existing process for glass waveguide fabrication113
4.2 Process for field assisted diffusion of silver ions in glass 114
4.3 Electrolytic process for releasing silver ions..115
4.4 Introduction of fritted glass around cathode in the electrolytic process 116
4.5 A concentration cell for measuring silver ion concentration 117
4.6 Glass bulb used in the reference electrode of the concentration cell 118
4.7 Measured and calculated Nernst potential for the concentration cell 119
4.8 Detailed schematic diagram for the electrolytic process 120

5.1 Prism coupler set up 134
5.2 Ray diagram for the prism coupler 135
5.3 Three prism method for loss measurement 136
5.4 Loss measurement at 0.6328 micron 137
5.5 Backscattering coefficient as a function of the atomic number 138

5.6 "Compo+Topo" photograph by the scanning electron microscope....139
5.7 Index profile of a planar glass waveguide fabricated by diffusion without applied field...140
5.8 Index profile of a planar glass waveguide fabricated by diffusion with applied field....141

6.1 Error contours....152
6.2 Δn-C_o curve for Labmate glass....153
6.3 Estimation of ΔN for Labmate glass....154
6.4 D-T curve for Labmate glass....155
6.5 Design curves for λ=0.6328 micrometer....156
6.6 Design curve for λ=1.32 micrometer....157

7.1 Set-up for measuring mode profiles in planar waveguides....153
7.2 Mode profile for the fundamental mode....164
7.3 Mode profile for the first mode....165
7.4 Mode profile for the second mode....166
7.5 Skewed index profile of a buried waveguide....167
7.6 Symmetric, fiber-like index profile of a buried waveguide....168
7.7 Photolithographic lift-off technique....169
7.8 Aluminum mask pattern for channel waveguide fabrication....170

Abstract of Dissertation Presented to the
Graduate School of the University of Florida
in Partial Fulfillment of the Requirements
for the Degree of Doctor of Philosophy

PASSIVE GLASS WAVEGUIDES FOR INTEGRATED OPTICS

By

RAJENDRA K. LAGU

May 1985

Chairman: Dr. V. Ramaswamy
Major Department: Electrical Engineering

Recently, glass waveguides have received considerable attention in the development of passive integrated optical components such as star and access couplers, wavelength multiplexers and demultiplexers. Passive glass waveguide components are attractive because they are compatible with optical fibers and potentially inexpensive. Being passive, they cannot be tuned electrooptically to compensate for fabrication errors. Thus, precise process control is essential to assure their reproducible fabrication within specified tolerances.

In this project, we have addressed the problem of the design and fabrication of glass waveguides with emphasis on "reproducibility."

A combination of theoretical analysis, numerical simulation and experimental investigation is used to achieve a basic understanding of diffusion and optical wave propagation in glass. Normalized propagation constants and field profiles are calculated numerically for highly asymmetrical graded index planar waveguides and graded index channel waveguides with arbitrary index profiles. One and two dimensional diffusion equations, with and without applied electric field, are solved numerically to determine the nature of the index profiles of the practical glass waveguides. The results of diffusion simulation are confirmed by experimental measurement of the index profile by a new and simple technique--scanning electron microscopy.

A novel electrolytic process is developed for releasing silver ions in molten sodium nitrate and a Galvanic cell type transducer is developed for in situ measurement of silver ion concentration.

Single mode planar glass waveguides with very low loss (0.2 dB/cm) are fabricated using the electrolytic process. Empirical relations linking the process and device parameters are derived and used subsequently to formulate a systematic procedure for fabricating single mode waveguides entirely in terms of the process parameters. Finally, symmetric, buried waveguides with a fiber-like index profile are fabricated using a two-step diffusion process.

CHAPTER ONE
INTRODUCTION

1.1 Optical Communication Systems

Achievement of low propagation loss has made the optical fiber waveguide a leading contender as the transmission medium for a number of present and future communication system applications. Optical fiber waveguides offer many significant advantages compared to other transmission media which utilize metallic conductors (e.g., twisted pair and circular and rectangular metallic waveguides). These include cost effective long distance transmission without repeaters, immunity to electromagnetic interference (EMI), absence of cross talk and ground loops, high bandwidth capabilities, small size and weight, high degree of intercept security and dielectric isolation between transmitter and receiver.

The foregoing desirable features of optical fibers have strongly stimulated efforts in associated technologies such as fiber cabling, long life solid state sources, high performance detectors, integrated optical couplers and modulators. These technological advances have propelled the fiber optics field which was in its infancy in the early 1970s into a major industry today. The ongoing commercial installations, field trials and laboratory research activities indicate that the fibers will continue to play a major role in future telecommunication and computer systems.

The basic functions of an optical communication system are illustrated by considering a typical system as shown in figure 1.1. The system is used for transmitting analog signals, e.g., speech or video signals or digital signals, e.g., data streams. The analog signals are sampled and coded using some modulation scheme such as Pulse Code Modulation (PCM) or Delta Modulation (DM). The modulator output is essentially a pulse train which is used to drive a laser diode to produce an identical train of light pulses. The optical fiber is used to transmit these light pulses to the receiving end where a photodiode is used to convert them back into electrical pulses. This is followed by demodulation to recover the analog signal. An optical fiber however has two mechanisms, viz. attenuation and dispersion, which can successively degrade the signal as it travels down the fiber. The impurities in the material of the fiber tend to absorb and scatter the light, thus causing attenuation of the optical pulses. On the other hand, the material and waveguide dispersion broadens the light pulses resulting in the possibility of causing inter-symbol interference. This necessitates the use of repeaters at regular intervals along the fiber, where the signal is detected, reshaped, and retransmitted.

The dotted boxes A and B shown in figure 1.1 represent a class of devices called the Integrated Optical devices which have been recently introduced in the conventional optical communication systems. Often they are true optical signal processing components, in the sense their inputs and outputs are optical signals. They can perform a variety of operations on light signals, e.g., multiplexing, demultiplexing and wavelength selective filtering. In the case of electrooptic signal processing applications, e.g., switches and modulators, an electrical signal containing the information is used to generate the modulated optical output. Introduction of these devices has considerably improved the performance of optical communication systems, as illustrated in figure 1.2. With the possibility of multiplexing and demultiplexing several wavelengths on the same fiber, the information carrying capacity of a single carrier optical communication system can be multiplied by the number of wavelengths used. This scheme is known as Wavelength Division Multiplexing (WDM). Another area where active research is going on is duplex transmission over fibers, also shown in figure 1.2. By using two different wavelengths in opposite directions, a single fiber can carry a two-way transmission between two stations.

The fiber-optics technology is expanding with giant strides in the development of fiber fabrication, fiber connectors, cabling and optical communication systems, Excellent review papers covering all these aspects are available in literature, for example, Miller et al. [Mi73], Giallorenzi et al. [Gi80].

1.2 Optical Computing

Researchers have been trying to design an all-optical digital computer for the past few years. As the present computer technology is approaching the speed limits imposed by the Si or GaAs microelectronics technology, an optical computer is expected to improve the performance by orders of magnitude. One problem confronting the state of the art supercomputers is that of interconnection bandwidth. As the system cycle time and pulse widths shrink, the bandwidth needed to preserve the rising and falling edges of the pulsed signals increases. This makes it necessary to have bulky, expensive, terminated co-axial connections. Attempts are also made to keep the interconnection length as small as possible. For example, CRAY-1 has a maximum interconnection length of 6 inches.

Optical components, in principle, provide a possible solution to this problem because of their large bandwidth and non-interfering propagation [Hu84]. Difficulties in realizing all optical logic devices, which are the building blocks of arithmetic-logic units (ALUs) and memories, have so far prevented a practical solution to this problem. Recently, however, a feasible design for optical AND and XOR gates with propagation delays as low as 10 picoseconds has been reported [Le83]. All optical memory devices using optical bistability have also been proposed [Sm81, Te81]. These devices use the interaction of guided waves with optical non-linearities of dielectric (electrooptic) materials. This indicates that integrated optical devices such as waveguides and directional couplers are likely to become the basic components for the hardware of the future optical computers. Architectures for such high speed optical computers have already been proposed [Te79b]. Their unique feature is the use of the Residue Number System which is capable of performing addition and multiplication without the necessity for carry operation. Calculations can therefore be performed in a fully parallel manner utilizing the extremely high speeds of optical computing elements. Besides telecommunications, integrated optical devices are expected to find a large number of applications in this new and exciting area.

1.3 Review of the Progress in Integrated Optics

The research in Integrated Optics has continued to progress over the past ten to fifteen years. It is based primarily on the fact that light waves can be guided by very thin layers of optical materials. Using such planar, layered films as well as shaping them into appropriate configurations, e.g., strip, raised ridge and buried channel, a variety of integrated optical components capable of performing a wide range of operations on light waves have been realized. These components being small and compact, their integration can lead to extremely efficient miniaturized optical circuits with low drive power requirements. As the light energy propagating in these devices is confined to small cross-sectional dimensions, phenomena produced by high intensity fields such as non-linear optical interactions can be observed at modest input power levels. This feature has added another new dimension to the research in the area of Integrated Optics. As the research is inter-disciplinary, involving a number of scientific and technological disciplines, its advancement is a direct result of contributions from investigators having different backgrounds. Thus engineers and scientists with interest in optics and microwaves, engineers and physicists in the areas of semiconductors, crystal and surface phenomena have often worked together to explore new ways to design and fabricate these devices.

There have been several review articles that deal with the principles of dielectric waveguides--for example, methods to couple energy into film waveguides [Ti71, Ko75], and guided wave devices for communication applications [Al81]. The research can be broadly divided into two categories (with the requisite overlaps).

1) Development of substrate materials and fabrication processes.
2) Development of new devices or new configurations for the existing devices.

A variety of substrate materials such as polymers, fused silica, soda-lime silicate glass, Pyrex glass, Lithium Niobate, Lithium Tantalate, Zinc Oxide, III – V Semiconductors, etc. have been used over the last decade. The associated fabrication processes include ion implantation, ion diffusion, thermal outdiffusion, metal indiffusion, sputter coating and surface layer growth.

Some of the early films capable of guiding light were reported by Goell and Standley. In their process, Corning 7059 glass was RF sputtered on a microscope slide to produce a waveguiding film [Go69a]. Many varnishes and epoxies have also been deposited on glass substrate to form waveguides. Ulrich and Weber have reported films of polyurethane, epoxy and photoresist made by deposition on glass slides [Ul72]. Ramaswamy and Weber have reported polymer films with adjustable refractive index [Ra73]. Proton implantation has been used by Schineller et al. to create waveguiding layers in fused silica [Sc68]. Kaminow and Carruthers have used outdiffusion of Li atoms to form waveguiding layers in $LiNbO_3$ and $LiTaO_3$ [Ka73]. Indiffusion of various transition metal elements has been used by Schmidt and Kaminow to form low loss planar waveguides in $LiNbO_3$ [Sc74]. Ion-exchange has been used to form waveguiding layers in soda-lime silicate glass--Giallorenzi et al. [Gi73], and borosilicate glass--Izawa and Nakagome [Iz72].

In these cases, the propagation loss of the waveguide and ease of fabrication have been the major criteria for accepting or rejecting a substrate material. From these considerations, Titanium diffusion in $LiNbO_3$ and ion-exchange in glass have become the most popular techniques for waveguide fabrication.

The devices have evolved from simple planar waveguides to complicated analog to digital converters. Successful fabrication of embedded strip (channel) waveguides (Martin [Ma73b], Standley and Ramaswamy [St74]) was a major step in the development of Integrated Optics because it paved a way to a score of useful devices. High speed switches using stepped $\Delta\beta$ reversal (Kogelnik and Schmidt [Ko76]), interferometers (Martin [Ma75]) and balanced bridge modulators (Ramaswamy et al. [Ra78]) were some of the devices developed in the late seventies.

The present thrust of research in devices is towards super high speed electrooptic modulators and fast electrooptic guided wave analog to digital converters (Taylor [Ta79a], Leonberger et al. [Le 82]). Another area of active research is device integration. The ability to efficiently couple light between a single mode fiber and a strip waveguide is essential for these devices to be incorporated into practical systems. Increasing efforts in reducing the coupling loss have resulted in the achievement of extremely low throughput loss. An insertion loss of as low as 1 dB for 1.3 cm long fiber-waveguide-fiber device at $\lambda = 1.32$ μm has been demonstrated (Ramaswamy et al. [Ra82]).

Primary phase of development in this exciting new field seems to be successfully completed. With the design of several integrated optical components and the improvement in coupling efficiency between these components and optical fibers, the next goal seems to be the integration (in a limited way) of several such components, e.g., modulators, multiplexers, couplers and demultiplexers on the same substrate to form functional sub-systems.

Figure 1.3 illustrates a transmitting end optical sub-system which typically represents box A of figure 1.1. At the transmitting end, an external modulator is required if a continuous wave (CW) laser is used as the light source. The choice of substrate material is restricted to one of those which exhibit electrooptic effect, e.g., $LiNbO_3$. To make the modulator efficient, i.e., to have a small drive voltage, the waveguide width is kept as small as possible. Typically in $LiNbO_3$ modulators, strip waveguides about 3-4 μm wide are used. To split the modulator output to several parallel channels, a star coupler is used as shown in figure 1.3. To reduce the interconnect losses between a 2-3 μm wide waveguide and a single mode fiber with a core diameter of about 6-10 µm, a tapered waveguide transition as shown in figure 1.3 is needed.

Figure 1.4 illustrates a typical receiving end sub-system representing box B in figure 1.1. Since at the receiving end, there is no need to modulate information, any passive substrate material such as glass can be used. The waveguide width is in the range of 8-10 µm which makes it compatible with a single mode fiber, thus eliminating a need for a tapered waveguide transition. Typical devices used in this sub-system include a wavelength filter and a star coupler as shown in figure 1.4

1.4 Project Definition

The majority of the devices described in the last section have been fabricated on a $LiNbO_3$ substrate using Titanium indiffusion. Since $LiNbO_3$ is an electrooptic material the refractive index of the guide and/or the surrounding region can be altered by the application of an electric field. This electrooptic tuning has been extremely useful in meeting the desired device specifications. For example, the center wavelength of a demultiplexing filter can be tuned electrooptically to the exact wavelength desired [A178]. Being a crystalline material, the cost of $LiNbO_3$ is prohibitive as the growth of its single crystal requires a carefully controlled process. In addition, it has a rather high refractive index ($\simeq 2.2$) as compared to that of an optical fiber ($\simeq$ 1.46), resulting in high interconnect losses due to Fresnel reflection at the interface between $LiNbO_3$ devices and optical fibers. Choice of an electrooptic substrate material such as $LiNbO_3$ is only essential where modulation or any other active operation, e.g., switching is desired. However, at the receiving end of an optical communication system, as there is no need to modulate any information, some inexpensive "passive" material such as glass could be considered. Refractive index of soda lime-silicate glass is around 1.5 making it compatible with optical fibers. In the absence of electrooptic effect, however, the "passive" devices made on glass cannot be tuned to compensate for the fabrication errors. Thus strict fabrication tolerances and precise process control are needed to meet the desired device specifications.

In 1972, Izawa and Nakagome first established the feasibility of using Sodium-Thallium ion exchange in glass for making graded index optical waveguides [Iz72]. Since then several sporadic attempts [St77, Ch80, Li82] to revive this technique have occurred, none of which, however, has resulted in reproducible fabrication of single mode waveguides. The process basically involves a bath containing a mixture of molten $AgNO_3$ and $NaNO_3$ in which soda-lime-silicate glass slides, about 1 mm thick, are suspended for Na^+-Ag^+ exchange. The exchange of sodium ions in the glass with the silver ions in the bath creates a surface layer of higher refractive index capable of guiding light. The existing process lacks control on some of its parameters and no attempts are made to improve the process yield.

In this project, an electrolytic ion release technique is investigated with emphasis on the "reproducibility" and "manufacturability" aspects of waveguide fabrication. The theoretical part of the research has been directed first, to the basic understanding of the Ag^+ diffusion (exchange) process. This is followed by the study of electromagnetic wave propagation in graded index planar glass films so that the expertise gained would facilitate the design of future optical components. The experimental work is aimed at the development of a controlled process for reproducible fabrication of single mode waveguides, followed by the characterization of these waveguides.

Since these devices are made by the diffusion process, the process parameters, such as diffusion temperature and time and Ag^+ concentration, affect the device parameters (waveguide width and index profile) which in turn decide the propagation characteristics (number of modes supported and their propagation constants). Thus, in order to make single mode waveguides with the same characteristics, it is necessary to find the links relating the process, device and propagation parameters. This work addresses this problem for the case of planar guides formed on the surface of glass substrates.

The overall problem is divided into the following four sub-areas of research:

1. Propagation analysis
2. Diffusion simulation
3. Development of the fabrication process
4. Waveguide characterization.

The subsequent chapters describe the work carried out in these areas.

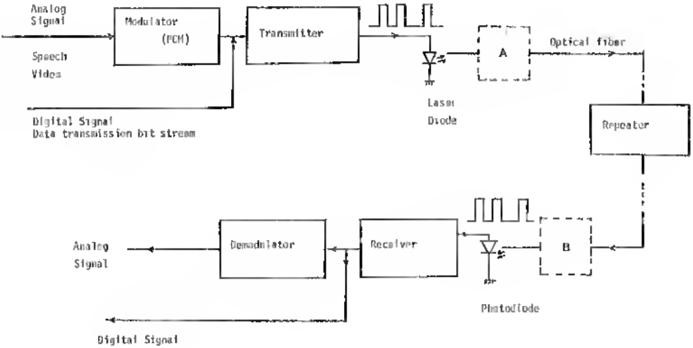
Analog
Signal
Speech
Video
Modulator
(PCM)
Digital Signal
Data transmission bit stream
Transmitter
Laser
Diode
A
Optical fiber
Repeater
B
Photodiode
Receiver
Demodulator
Analog
Signal
Digital Signal

Figure 1 1 An optical communication system

Wavelength Division Multiplexing

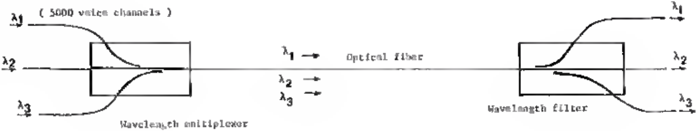
(5000 voice channels)
λ_1
λ_2
λ_3
Wavelength multiplexer
λ_1 →
λ_2 →
λ_3 →
Optical fiber
Wavelength filter
λ_1
λ_2
λ_3

Duplex transmission over optical fibers

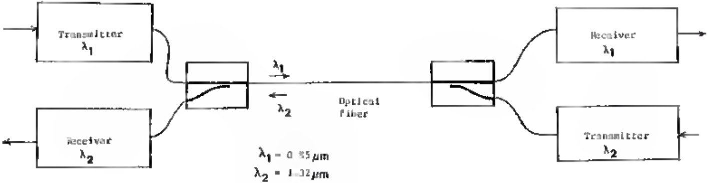
Transmitter λ_1
Receiver λ_2
λ_1
λ_2
Optical fiber
Receiver λ_1
Transmitter λ_2
λ_1 = 0.85 μm
λ_2 = 1.32 μm

Figure 1.2 Wavelength division multiplexing

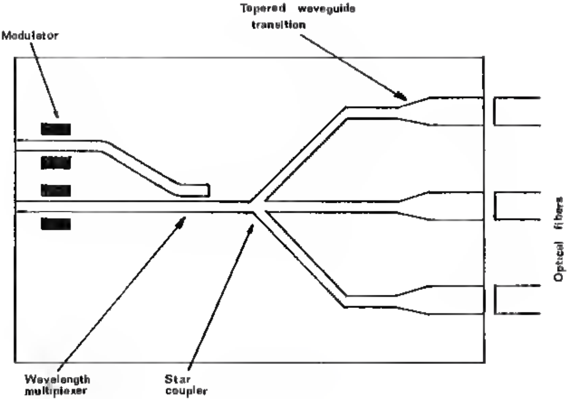
Tapered waveguide transition
Modulator
Optical fibers
Wavelength multiplexer
Star coupler

Figure 1.3 Transmitting end subsystem

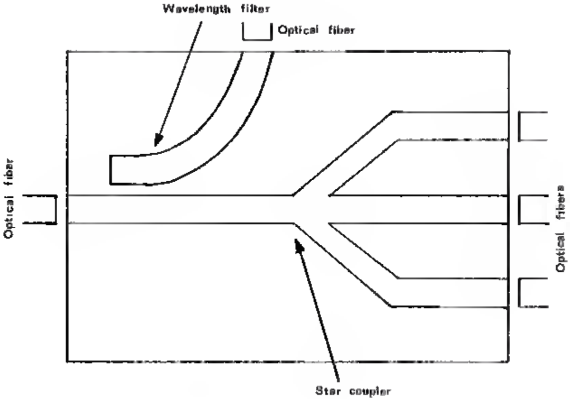
Wavelength filter
Optical fiber
Optical fiber
Optical fibers
Star coupler

Figure 1.4 Receiving end subsystem

CHAPTER 2
PROPAGATION ANALYSIS

Propagation analysis of dielectric waveguide mainly consists of determining the number of modes supported by the waveguide, the mode propagation constants, and the transverse field distribution associated with these modes. This information is essential for the design of almost all type of integrated optical components. In end-fire couplers, the end faces of waveguides and/or fibers are polished and joined with or without an index matching fluid in between. The coupling efficiency depends upon the spatial overlap of the fields in the two waveguides. Thus, to achieve good efficiency, the field profile in these guides should have similar shape and dimensions. Hence, to reduce the coupling loss, accurate knowledge of field profiles in both of these guides is essential. In directional coupler-type devices, the waveguides are brought adjacent to each other sideways and the coupling takes place through the interaction of the evanescent fields due to the traveling waves in the guides. This is also referred to as "optical tunneling." Complete energy transfer can occur only when the propagation constants of the modes are the same. Thus, determination of the mode propagation constants and their relationship to the device parameters are necessary for efficient device design.

Graded index structures are important because most of the waveguides are formed in practice by diffusion which results in waveguides with graded refractive index transverse to the direction of propagation. Different diffusion conditions manifest themselves in different index profiles. For example, one-dimensional diffusion with an infinite source of dopant results in a complementary error function profile. On the other hand, an exhaustible input source, i.e., the dopant source that is depleted entirely during diffusion, yields a Gaussian index profile [So63]. For the waveguides formed by sputter deposition, the profile is essentially like a step index [Go69e].

The following two types of guides, which occur in practice, are considered in detail in the subsequent sections.

1. Planar Step Index Waveguides
2. Planar Graded Index Asymmetrical Waveguides

2.1 Planar Step Index Waveguides

The step index waveguide, shown in figure 2.1, consists of three layers: substrate, film and cover (or superstrate). Often the superstrate is air, unless some other material is used to coat the waveguide as is the case with polymer clad waveguides. The guided mode propagation can be understood in terms of a ray picture as shown in figure 2.1. A ray travels in a zig-zag fashion inside the film undergoing total internal reflections at the film-substrate and film-cover boundaries (points A and B respectively). As long as angle θ exceeds the critical angle for both these interfaces, the ray will be confined in the film and guided along z direction. In addition, the ray has to satisfy a condition called the "transverse resonance condition." For a given film only a finite number of rays meet this condition and as a result the film supports a finite number of modes. The transverse resonance condition is outlined below.

2.1.1 Nomenclature

n_f = film refractive index
n_c = cover refractive index
n_b = substrate refractive index (bulk index)
λ_o = free space wavelength
k_o = $2\pi/\lambda_o$ = free space propagation constant
$k_o n_f$ = magnitude of the wave vector in the film
β = $k_o n_f \sin\theta$ = propagation constant in z direction
κ_f = $k_o n_f \cos\theta$ = transverse propagation constant
ϕ_s = phase shift at the total internal reflection at the film-substrate interface
ϕ_c = phase shift at the total internal reflection at the film-cover interface
N = β/k_o = mode index

2.1.2 Ray Analysis

As the ray travels through path ABC in figure 2.1, it suffers phase shifts at both interfaces due to total internal reflection as well as a phase change while propagating inside the film. If the total accumulated phase change is an integral multiple of 2π, then the phase front after total internal reflection at A as it advances to C comes in phase with the phase front which is reflected at C, resulting in a constructive interference. Under these conditions, the film supports a ray corresponding to a specific angle θ. For a given set of film parameters, the rays propagate at specific discrete angles. This transverse resonance condition can be written as

$$2\kappa_f d + \Phi_s + \Phi_c = 2m\pi \ , \tag{2.1}$$

where m is an integer and the phase shifts Φ_s and Φ_c can be expressed in terms of film parameters [Ti71,Ko79]. For TE modes with the electric field polarization parallel to the plane of the film,

$$\Phi_s = -2 \tan^{-1}[(n_f^2 \sin^2 \theta - n_s^2)^{1/2} / n_f \cos \theta] \tag{2.2}$$

$$\Phi_c = -2 \tan^{-1}[(n_f^2 \sin^2 \theta - n_c^2)^{1/2} / n_f \cos \theta] \tag{2.3}$$

For TM modes with the magnetic field parallel to the plane of the film, the arguments within the square brackets in equations (2.2) and (2.3) are multiplied by the quantity $(n_f/n_s)^2$ and $(n_f/n_c)^2$ respectively.

The values of Φ_s and Φ_c from equations (2.2) and (2.3) can be inserted into equation (2.1) which then can be solved for κ_f using iterative procedure and the value of β can be found from κ_f. There are five independent variables in this problem, namely, n_c, n_f, n_b, d, and λ_o which decide the value of κ_f and β. Kogelnik and Ramaswamy [Ko74] have shown that the number of independent parameters can be reduced by introducing appropriately normalized parameters. The associated scaling rules then provide universal plots from which the mode index can be determined for any slab waveguide configuration.

The following normalized, dimensionless parameters are defined:

$$V = \frac{2\pi}{\lambda_o} d \left(n_f^{2} - n_b^{2}\right)^{1/2} \tag{2.4}$$

This parameter, usually referred to as "V number" has the requisite information regarding the waveguide geometry and refractive indices and the wavelength of operation. Thus, this parameter is defined by combining all the independent parameters.

The dependent parameter, namely the mode index N, has been normalized as the b parameter

$$b = \frac{N^2 - n_b^{2}}{n_f^{2} - n_b^{2}} \tag{2.5}$$

As N varies between n_b and n_f, b takes values between 0 and 1. An asymmetry parameter a is also defined. For TE modes

$$a_E = \frac{n_b^2 - n_c^2}{n_f^2 - n_c^2} \tag{2.6}$$

For TM modes

$$a_M = \left(\frac{n_f^4}{n_c^4}\right)\left(\frac{n_b^2 - n_c^2}{n_f^2 - n_b^2}\right) \tag{2.7}$$

For symmetric waveguides, the cover and substrate have the same refractive index, i.e., $n_b = n_c$ making $a = 0$. For a highly asymmetrical case, $n_f \approx n_b$ and $n_c \ll n_f$ thus, $a \to \infty$. Using these parameters, equation (2.1) can be written as

$$V(1-b)^{1/2} = \tan^{-1}[b/(1-b)]^{1/2} + \tan^{-1}[(b+a)/(1-b)]^{1/2} + m\pi \tag{2.8}$$

Equation (2.8) is a normalized version of the transverse resonance condition and indicates that the normalized guide index b depends only on V and a. This equation is solved for m = 0,1,2, i.e., the first three modes for various values of a from 0 to ∞ and the results are plotted in figure 2.2. For TE and TM modes, a is given by equations (2.6) and (2.7) respectively. These curves are called the b-V characteristics for the step-index waveguide, which are similar to β-ω diagrams of the rectangular metallic waveguides; however, these plots are universal in that they represent normalized propagation for both TE and TM modes. This makes them helpful in the step index waveguide design.

2.2 Planar Asymmetrical Graded Index Waveguide

The model for a planar, asymmetrical graded index waveguide is shown in figure 2.3. The index profile of a graded index waveguide occupying the half space $(x > 0)$ is given by

$$n(x) = n_b + \Delta n\, f(x) \tag{2.9}$$

where

$\Delta n = n_s - n_b$

n_b = bulk refractive index

n_s = surface refractive index

$f(x)$ = index profile function.

The index profiles for various possible functions $f(x)$ are plotted in figure 2.4.

Profile	$f(x)$
Complimentary error	$\mathrm{erfc}(x)$
Gaussian	e^{-x^2}
Exponential	e^{-x}
Quadratic	$1 - x^2$
Linear	$1 - x$

The nature of f(x) depends on the fabrication process.

2.2.1 Normalization-Dispersion Equation

The modal analysis of the graded-index waveguide can be done almost on the same lines as the step index except that the step index waveguides has zig-zag rays with two total internal reflections where as in graded index guides the rays follow curved paths with a total internal reflection occurring at the cover-film interface and a turning point occurring inside the graded index film as shown in figure 2.3.

The transverse propagation constant κ_f, however, is a function of x. The transverse resonance condition for this case is given by the integral

$$2 \int_0^{x_t} \kappa_f(x)\, dx + \phi_c + \phi_t = 2m\pi \tag{2.10}$$

This is also referred to as the dispersion (or characteristic) equation. Here, ϕ_t is the phase shift encountered at the turning point x_t. Hocker and Burns [Ho75] have shown that $\phi_t = -\pi/2$ by considering the phase change in the limit $\theta(x) \to \pi/2$. The phase shift ϕ_c, upon total internal reflection at the cover-guide interface, is given by equation (2.3).

The dispersion equation (2.10) can be normalized as follows:

The following parameters are defined:

$x' = x/d$ = normalized depth

$n(x') = n_b + \Delta n\ f(x')$

The same definitions for b and V can be used (equation (2.4) and (2.5)) with the film index n_f changed to n_s, representing the surface index. When $\Delta n << n_b$ (which is a valid assumption for practical case),

$$V = k_o d\ (2n_b\ \Delta n)^{1/2}$$

For a highly asymmetrical case, $n_o << n_s$. Also for practical waveguides, $\Delta n << n_b$ so that $n_s = n_b$.

The rays in these waveguides are almost on axis, so that $\theta = \pi/2$. Thus, $\sin\theta = 1$ and $\cos\theta = 0$. Substituting these expressions in equation (2.3), we get $\phi_c = -\pi$.

Using these approximations and normalizations, the integral equation (2.10) can be converted to

$$V \int_0^{x'_t} [f(x') - b]^{1/2} dx' = (m + 3/4)\ \pi \qquad (2.11)$$

At the turning point x_t, the wave vector is in the direction of propagation (figure 2.3). Therefore, $\kappa(x_t) = 0$. However, as seen in figure 2.3,

$$\kappa(x) = (k_o{}^2 n^2(x) - \beta^2)^{1/2} \qquad (2.12)$$

Thus, at the turning point

$$k_0 n(x_t) = \beta \qquad (2.13)$$

Since $\beta = k_0 N$, at the normalized turning point x_t', $n(x_t') = N$.

Now by definition of $n(x')$,

$$n(x_t') = n_b + \Delta n \ f(x_t')$$

when $\Delta n << n_b$,

$$n^2(x_t') = N^2 = n_b^2 + 2\Delta n \ f(x_t') \ n_b \ ,$$

so,

$$f(x_t') = \frac{N^2 - n_b{}^2}{2n_b \ \Delta n} = b \qquad (2.14)$$

Equation (2.11) and (2.14) are solved numerically to find the b-V characteristics of graded index waveguides. For a given index profile $f(x')$, a value of b is assumed and from equation (2.14), x_t' is calculated. The value of x_t' is used in equation (2.11) to evaluate the integral numerically. Then for a given mode order m, the value of V is calculated.

The b-V characteristics for the fundamental mode corresponding to various index profiles (figure 2.4) are shown in figure 2.5.

2.2.2 Normalization--Field Equation

To calculate the field profiles, Maxwell's equations are solved with appropriate boundary conditions. The transverse field components for TE modes can be shown to satisfy the transverse Helmholtz equation [Ti71],

$$\frac{d^2E_y}{dx^2} + (k_o^2n^2(x) - \beta^2)\ E_y = 0 \tag{2.15}$$

Depending upon the index profile n(x), this second-order differential equation has been solved in the past by different techniques. Conwell has considered an exponential profile and has obtained a closed form analytical solution in terms of Bessel functions [Co74]. Marcuse has approximated an arbitrary index profile by two piecewise linear segments and has shown that the mode profile can be expressed in a closed form as a combination of Bessel functions [Ma73a]. For a quadratic index profile, this equation takes the form of one-dimensional Schroedinger equation for a quadratic potential well and the solution is similar to that of a quantum mechanical harmonic oscillator [Ko79]. The closed form solution is expressed in the form of Hermite-Gaussian functions. Smithgall and Dabby have used numerical techniques to solve the differential equation for the complementary error function profile [Sm73].

The analytical techniques provide closed-form solutions for simple amenable profiles such as quadratic and exponential but cannot be easily extended to more useful Gaussian and erfc profiles. Some of the closed-form solution, e.g., for exponential profile, involve Bessel functions of arbitrary order, $J_{1.7}(x)$, $J_{3.8}(x)$, etc., which are difficult to evalute and there are no tables readily available. The numerical techniques, on the other hand, are fairly straightfoward, but the solution applies to specific cases and recomputation is necessary each time the waveguide parameters are changed.

If the differential equation (equation (2.15)) is normalized prior to the application of the numerical method, then the solution becomes fairly general in the sense that it is applicable to all waveguides with that particular index profile [Ra83]. By changing the variable from x to x' = x/d and by using the usual definitions for the normalized variables, equation (2.15) can be normalized as shown below.

The derivatives can be expressed as

$$\frac{dE}{dx} = \frac{dE}{dx'} \cdot \frac{dx'}{dx} = \frac{1}{d}\frac{dE}{dx'}$$

so

$$\frac{d^2E}{dx^2} = \frac{1}{d^2}\frac{d^2E}{dx'^2}$$

Now

$$n(x) = n_b + \Delta n\ f(x)$$

when $\Delta n << n_b$,

$$n^2(x) = n_b^{\,2} + 2\Delta n\, n_b\, f(x)$$

From equation (2.4) with small index approximation,

$$V = k_0 d(2n_b\, \Delta n)^{1/2}$$

Also, $\beta = k_0 N$.

Using these approximations, we get

$$\frac{d^2E_y}{dx'^2} + V^2[f(x') - b]\; Ey = 0 \tag{2.10}$$

The results are applicable to TM modes as well except that E_y is replaced by H_y.

2.2.3 Numerical Solution

The differential equation can be modelled as a two-point boundary value problem. From physical considerations, the field $E_y(x')$ must approach 0 as $x' \to \infty$, imposing the boundary condition $E(\infty) = 0$. In order to reduce the number of numerical computations, the field can be assumed to vanish at some finite x'. For well guided modes, $x' = 2$ seems to be sufficiently deep for the assumption that the field vanishes at this point. Obviously, for higher order modes and for modes with V number closer to cut-off, this value needs to be increased appropriately. Thus, the first boundary condition is $E(2) = 0$. For the second boundary condition, a unit field can be assumed at the cover-guide interface without loss of generality, because the solution of this homogeneous, linear differential equation is unique up to a constant multiplier. (This means if $E_y(x')$ is a solution of equation (2.16), then so is $pE_y(x')$, where p is a scalar.) Thus, the second boundary condition is $E(0) = 1$.

With these boundary conditions, the two-point boundary value was solved using a fourth order Runge-Kutta method. Since for quadratic index profile, the solution exists in closed form as Hermite-Gaussian functions [Ko79], this profile was used to verify the results of our numerical method. The numerical results were in excellent agreement with the exact analytical results, establishing the validity of the method. It was then extended to the more useful Gaussian and complementary error function profiles. Figure 2.6 shows the b-V characteristics for the first three modes of the Gaussian profile. Figure 2.7 shows the normalized field profiles for the fundamental mode for various V values: V = 5, 10 and 15. As expected, for higher V number, better mode confinement is obtained. The peak of the modal amplitude profile shifts toward the cover-guide interface with increasing V. Figure 2.8 shows the profiles for m = 0, 1, and 2 for a multimoded waveguide with a large V number, V = 18. The modes in the plot are normalized to carry equal power. It is seen that the peaks of the higher order mode occur well inside the waveguide, and thus, most of the energy is confined to the region further away from the surface. This confirms the experimental observation that the fundamental mode of graded index planar waveguides, though more tightly guided compared to the higher order modes, shows higher propagation loss in guides with serious surface imperfections as it is more prone to surface scattering loss [Re75]. A similar exercise was carried out for the complementary error function index profile and the results are plotted in figures 2.9, 2.10 and 2.11.

Since the mode profiles are normalized, it is possible to define a normalized modal width W' = W/d where W is the distance between two points of the modal profile where the intensity falls to 1/e of its peak value and d is the effective diffusion depth. Since W' only depends on V number, it is plotted in figures 2.12 and 2.13 as a function of V for Gaussian and erfc profile respectively. While designing a single mode waveguide of a specified modal width, this universal curve can be used. As seen in figure 2.12, a Gaussian index profile waveguide is single moded for V numbers between 1.9 and 4.4. For a given single mode fiber with a Gaussian intensity distribution of known width W_F, this curve can be used to select the V number and the diffusion depth in the single mode regime so that

$W'd = W_f$. This choice of V number will result in efficient end-fire coupling between the fiber and the waveguide.

To understand how index profile affects the field profile, several waveguides with different index profiles such as linear, quadratic, exponential, Gaussian erfc and step were considered. The V number for all of them was equal to 8. The field profiles of the fundamental mode were calculated numerically and plotted as shown in figure 2.14. It is seen that though the step index waveguide shows a markedly different mode profile, all other graded index guides essentially have the same mode profile and, therefore, essentially have the same normalized effective modal width W'. This can be understood by considering the normalized differential equation (2.16). For a given V number, the solution to this equation depends on the coefficient $(f(x') - b)$. Figures 2.4 and 2.5 indicate that for profiles with higher values of refractive index $f(x')$ at any x' also have a larger b for given V so that the difference $(f(x') - b)$ is approximately constant for all the profiles. This result has significant implications in the design of fiber-guide end-fire couplers because it indicates that modal width, while somewhat sensitive to the V number, is surprisingly insensitive to the index profile. Tailoring of the index profile, therefore, does not seem to be as important in coupler design as is maintaining the required V number. As pointed out earlier, the profiles are determined by the diffusion process. In practice, it is very difficult to maintain either an infinite source of dopants or to completely exhaust it in time prior to the completion of diffusion. Thus, the profile may be somewhere between Gaussian and erfc. The above result indicates that achievement of a specific index profile is not absolutely necessary for single mode applications. However, the selection of V number in conjunction with the diffusion depth, which can be achieved only through careful control of the diffusion process, is extremely important.

2.3 Planar Graded Index Buried Waveguides

Buried waveguides fabricated in glass by a two-step diffusion process have a skewed index profile [Ch80] which can be approximated by two linear segments as shown in figure 2.15.

For propagation analysis, the following parameters are defined:

$x' = x/d$ = normalized depth

$n_p = (n_b + \Delta n)$ = peak refractive index

n_b = bulk refractive index

d = waveguide depth

Let x_p be the depth at which the peak refractive index n_p occurs, so that

$$0 \leq x_p \leq d$$

We define

$$r = x_p/d$$

Thus,

$$0 \leq r \leq 1$$

The usual definitions for V and b parameters are considered (equation 2.4 and 2.5), except that the film refractive index n_f is replaced by the peak refractive index n_p.

As seen from the ray picture in figure 2.15, there are two turning points for a ray corresponding to a well guided mode.

The transverse resonance condition for this case can be written as a modification of equation (2.11) as

$$2V \int_{x'_{t1}}^{x'_{t2}} \sqrt{f(x') - b}\, dx' + \phi_{t1} + \phi_{t2} = 2m\pi \qquad (2.17)$$

where ϕ_{t1} and ϕ_{t2} are the phase shifts at the normalized turning point x'_{t1}, x'_{t2} (figure 2.15), which are equal to $-\frac{\pi}{2}$ as described in the previous section.

This equation can be split as

$$V(\int_{x'_{t1}}^{r} \sqrt{f_1(x') - b} \; dx' + \int_{r}^{x'_{t2}} \sqrt{f_2(x') - b} \; dx' = \frac{(2m+1)\pi}{2} \qquad (2.18)$$

But f_1 and f_2 are two linear functions,

$$f_1(x') = x'/r \qquad (2.19)$$

$$f_2(x') = (1 - x')/(1 - r) \qquad (2.20)$$

At the turning points, as shown in the equation (2.14),

$$f_1(x'_{t1}) = f_2(x'_{t2}) = b$$

Thus,

$$x'_{t1} = br \quad \text{and} \quad x'_{t2} = 1 - b(1 - r)$$

Substituting $f_1(x')$ and $f_2(x')$ as given by equations (2.19) and (2.20) into equation (2.18), we get

$$\frac{2V}{3}(1 - b)^{3/2} = \frac{(2m+1)\pi}{2} \tag{2.21}$$

$$b = 1 - [\frac{3(2m+1)\pi}{4V}]^{2/3} \tag{2.22}$$

It is interesting to note that the b-V characteristic comes out as a closed form expression in which r, which is the normalized location of the peak of the index profile, does not appear at all.

Thus, for well guided modes of a triangular index profile waveguide (with their energies in the peak index region), the propagation characteristics are independent of the location where the peak index occurs. In figure 2.16, the b-V characteristics for the first three modes, m = 0, 1, 2, are plotted. Comparison of figures 2.6, 2.9 and 2.16 indicates that, compared to waveguides with Gaussian or erfc profiles, a buried triangular waveguide remains single modal over a larger range of V number.

2.4 Graded Index Channel Waveguides

Throughout the development of integrated optical devices, channel waveguides have played a major role because they form the basis for the design of optical components such as directional couplers, modulators, switches, etc.

The analysis of the modal disperson in graded index channel waveguides is, therefore, an important problem and a number of methods for both step and graded index channel waveguides are reported in the literature. Goell has used circular harmonic numerical analysis for a step index channel immersed in an infinite medium of lower index [Go69b]. Marcatili has analyzed the step index channel surrounded by four different refractive index media by ignoring the fields in the corner region [Ma69]. Literature on graded index channels includes Effective Index method of Hocker and Burns [Ho77], Yeh's Finite Element method [Ye75], Pichot's method based on Vector Integral equations [Pi82], and Matsuhara [Ma73c] and Taylor's [Ta76] Variational method.

All these methods suffer from the lack of generality in the sense that the solutions are applicable only to the specific waveguides and extensive recomputation is necessary if the waveguide parameters are changed. Normalization of the scalar Helmholtz equation prior to its numerical solution is expected to make the solutions fairly general.

A new method called a "Variational-Finite difference" method is formulated to analyze graded index channel waveguides with arbitrary index profiles and aspect ratios [La84a]. The method has the following advantages.

i. It can accept any index profile, even if it is available at discrete points. The method, therefore, can directly use the results of diffusion simulation where the index profile is obtained at discrete points from the numerical solution of the two-dimensional diffusion equation.

2. It accepts various waveguide aspect ratios without any additional reformulation. This feature is important because the aspect ratio of a practical waveguide depends on both the diffusion depth and waveguide width, which in turn depends on the lateral diffusion. Thus, the aspect ratio usually has a value other then unity.
3. The method solves the normalized Helmholtz equation, so that the results are applicable to all waveguides as long as the index profile remains the same.

2.4.1 Theory

The dielectric channel waveguide under consideration is shown in figure 2.17. In the practical case of channels formed by diffusion, there are no sharp boundaries between the waveguide and the substrate as shown in figure 2.17, so the width w and the depth d should be replaced by the effective width and the effective depth respectively.

The index profile can be expressed as

$$n(x,y) = n_b + \Delta n\ f(x,y) \qquad (2.23)$$

where $f(x,y)$, as before, is the normalized index profile function and has a value between 0 and 1.

For the substrate region, $n(x,y) = n_b$, so $f(x,y) = 0$.

Where $f(x,y) = 1$, $n(x,y) = n_b + \Delta n = n_p$, the peak refractive index.

For small index difference ($\Delta n << n_b$), the modes supported by this type of waveguide can be divided into two groups:

1. Quasi-TE modes in which the main field components are E_x and H_y.
2. Quasi-TM modes in which the main field components are E_y and H_x.

For quasi-TE modes, the field E_x can be expressed as

$$E_x = E(x,y)e^{-j\beta z} \qquad (2.24)$$

where the field amplitude $E(x,y)$ satisfies the two-dimensional scalar Helmholtz equation

$$\frac{\partial^2 E}{\partial x^2} + \frac{\partial^2 E}{\partial y^2} + [K_0^2 n^2(x,y) - \beta^2]E = 0 \qquad (2.25)$$

The following normalized space variables are defined.

$x' = x/w$ = normalized width

$y' = y/d$ = normalized depth (2.26)

$r = w/d$ = aspect ratio

The V and b parameters are defined as usual (equations (2.4) and (2.5)) except that the film index, n_f, is replaced by peak index, n_p.

As explained in section 2.2.2, these normalized variables can be used to convert the scalar Helmholz equation (2.25) into a normalized partial differential equation

$$\frac{1}{r^2}\frac{\partial^2 E}{\partial x'^2} + \frac{\partial^2 E}{\partial y'^2} + V^2[f(x',y') - b]E = 0 \qquad (2.27)$$

2.4.2 Variational Formulation

Define a scalar functional

$$\phi = \iint_D F\left(E, \frac{\partial E}{\partial x'}, \frac{\partial E}{\partial y'}, x', y'\right) dx'dy' \qquad (2.28)$$

where x', y' are the independent variables and E is the dependent variable. The integration is over domain D in the (x',y') plane and the boundary of the domain D is considered fixed for all variations. The surface $E(x',y')$ which extremizes the function ϕ, is given as a solution of the Euler-Lagrange equation [Ir59]:

$$\frac{\partial F}{\partial E} - \frac{\partial}{\partial x'}\left(\frac{\partial E}{\partial p}\right) - \frac{\partial}{\partial y'}\left(\frac{\partial E}{\partial q}\right) = 0 \qquad (2.29)$$

where $p = \frac{\partial E}{\partial x'}$ and $q = \frac{\partial E}{\partial y'}$.

At the minimum of ϕ, $\delta\phi = 0$.

If we choose

$$F = V^2 f(x',y')\ E - \frac{1}{r^2}\left(\frac{\partial E}{\partial x'}\right)^2 - \left(\frac{\partial E}{\partial y'}\right)^2 - V^2 bE^2 \qquad (2.30)$$

then the Euler-Lagrange equation for this choice of F becomes the normalized Helmholtz equation (2.27).

Thus any $E(x',y')$ which minimizes ϕ is the solution of equation (2.27) and hence is the field profile of the channel waveguide. The variational formulation thus converts the problem of solving the partial differential equation (2.27) to the problem of minimizing function ϕ given by

$$\phi = \int_D\int \{V^2 f(x',y')E^2 - \frac{1}{r^2}\left(\frac{\partial E}{\partial x'}\right)^2 - \left(\frac{\partial E}{\partial y'}\right)^2 - V^2 bE\}^2 dx'dy' \qquad (2.31)$$

The domain D extends ideally from $-\infty$ to ∞ in both width and depth directions because, theoretically, the field vanishes at infinity. However, without loss of accuracy, from practical considerations, a smaller region around the waveguide can be chosen, on the boundary of which, the field can be assumed to be effectively zero.

Define the functionals I and J as

$$I = \int\int_D [V^2 f(x',y')E^2 - \frac{1}{r^2}(\frac{\partial E}{\partial x'})^2 - (\frac{\partial E}{\partial y'})^2]dx'dy' \qquad (2.32)$$

$$J = \int\int_D E^2 dx'dy' \qquad (2.33)$$

Thus

$$\phi = I - (V^2 b)\ J \qquad (2.34)$$

At the minimum, $\delta\phi = 0$, so that

$$\delta I - (V^2 b)\ \delta J = 0 \qquad (2.35)$$

We define a scalar function λ given by

$$\lambda = I/J \qquad (2.36)$$

This function attains a stationary value λ^* when

$$\delta\lambda\Big|_{\lambda^*} = 0 \qquad (2.37)$$

But

$$\delta\lambda = \frac{J\delta I - I\delta J}{J^2} \qquad (2.38)$$

Thus,

$$J\delta I - I\delta J = 0 \qquad (2.39)$$

$$\delta I - (I/J)\delta J = 0 \qquad (2.40)$$

$$\delta I - (\lambda^*)\delta J = 0 \qquad (2.41)$$

Comparing equations (2.35) and (2.41),

$$\lambda^* = v^2 b \qquad (2.42)$$

Thus the minimum of ϕ can be found by finding the stationary value of I/J.

To proceed further, it is necessary to make an approximation for the functional form of the field distribution E(x',y') and then use the variational approach to find the undetermined coefficients in the functional form.

Matsuhara [Ma73c] and Taylor [Ta76] have expressed E(x,y) as a linear combination of a finite number of parabolic cylinder functions

$$E(x,y) = \sum_{i,j} a_{ij} [2\pi\xi\eta i!j! \; D_i(x/\xi) D_j[(y-y_0)/\eta] \qquad (2.43)$$

where D_i and D_j are parabolic cylinder functions of the order i and j respectively.

To make the numerical realization easier, a new form of function is chosen using the finite-difference approach. As shown in figure 2.18, the waveguide ABCD is surrounded by a boundary PQRS where the field is assumed to vanish. For well guided modes the field attains a negligibly small value at distances about twice the waveguide dimensions so that this assumption is justified. Obviously for modes closer to cut-off, the distance needs to be increased much further.

A square grid is drawn inside the box and the field $E(x',y')$ is defined at the grid points. Inside the grid, the field is expressed as a bilinear interpolation of the grid point values [Fo60]. In figure 2.19, a typical square in the box is expanded and the field distribution for this square is written as

$$E(x',y') = \frac{1}{h^2}[E_{hh}x'y' + E_{oo}(h - x')(h - y') +$$

$$E_{ho}x'(h - y') + E_{oh}(h - x')y'] \qquad (2.44)$$

Since this form of interpolation is linear on each link of the net, it provides $E(x',y')$ which is continuous on the whole region. If we select $E(x',y')$ to vanish at nodes on the boundary PQRS, then it automatically satisfies the boundary condition.

2.4.3 Numerical Solution

The integral functions I and J defined by equations (2.32) and (2.33) can be expressed as summations.

For example, for J

$$\iint\limits_{\substack{\text{Rectangle}\\ \text{PQRS}}} E^2(x',y')\,dx'dy' = \sum \iint\limits_{S_h} E^2(x',y')\,dx'dy' \qquad (2.45)$$

where S_h is a single square with sides h.

For a single square,

$$\iint\limits_{S_h} E^2(x',y')\,dx'dy' = \iint\limits_{S_h} \frac{1}{h^4}\,[E_{hh}x'y' + E_{ho}x'(h-y') +$$

$$E_{oo}(h-x')(h-y') + E_{oh}(h-x')y']^2\,dx'dy'$$

$$= \frac{h^2}{9}\,(E_{oo}^2 + E_{ho}^2 + E_{oh}^2 + E_{hh}^2 + E_{oo}E_{ho} + E_{oh}E_{oo} +$$

$$E_{hh}E_{ho} + E_{hh}E_{oh}) + \frac{h^2}{18}\,(E_{oo}E_{hh} + E_{ho}E_{oh}) \qquad (2.46)$$

Thus, a vector U is defined whose entries are the values of $E(x',y')$ at the grid points; then the summation in equation (2.45) can be written as a quadratic form

$$J = \iint_{\substack{\text{Rectangle}\\ \text{PQRS}}} E^2(x',y')\, dx'dy' = U^T BU \tag{2.47}$$

where B is a real symmetric matrix.

A similar approach is taken for the numerator integral I, except that in this case, the index profile $f(x',y')$, which appears in the expression, is also expressed as a bivariate linear interpolation of its grid point values.

Thus equation (2.36) becomes

$$\lambda = I/J = (U^T AU)/(U^T BU) \tag{2.48}$$

To find λ^*, the stationary value of λ,

$$\frac{\partial \lambda}{\partial U} = 0 \tag{2.49}$$

which gives the condition

$$AU = \lambda BU \tag{2.50}$$

Premultiplying by B^{-1},

$$(B^{-1}A)U = \lambda U \tag{2.51}$$

Now b is the normalized propagation constant with $0 < b < 1$, so that λ takes values between 0 and V^2. Thus, only those real eigenvalues of the matrix $(B^{-1}A)$ which are between 0 and V^2 correspond to the modes of the waveguide.

For numerical computation of the eigenvalues of a matrix, simple algorithms are available to find the largest eigenvalue, such as the power method. This method is modified to find the eigenvalues between the range $0 - V^2$ as follows.

In general, for any matrix A, if $\mu_1, \mu_2, \mu_3, \ldots, \mu_4$ are its eigenvalues with eigenvectors $U_2, U_2, U_3, \ldots, U_N$, then the matrix $(A-mI)^{-1}$ has the same eigenvectors corresponding to the eigenvalues $(\mu_i - m)^{-1}$.

Thus if $|m - \mu k|$ is less than $|m - \mu l|$ for $i \neq k$, then $(\mu_k - m)^{-1}$ dominates the other $(\mu_i - m)^{-1}$ and hence the power method, applied to $(A-mI)^{-1}$, converges to the eigenvalue $(\mu_k - m)^{-1}$.

From the physical considerations, a reasonable estimate of the value of b is available for a given waveguide. For example, the fundamental mode has its b closer to 1 than that of any other mode.

Thus,

$$\lambda^*_{\text{estimated}} = (V^2)(b_{\text{estimated}})$$

This estimated value of λ^* can be used in the modified power method. The algorithm can handle arbitrary aspect ratios as follows.

Consider the integral I as given by the equation (2.32). It can be split as the sum of three integrals so that

$$I = \iint_D V^2 f(x',y') \mathcal{E}^2 dx'dy' - \frac{1}{r^2} \iint_D \left(\frac{\partial \mathcal{E}}{\partial x'}\right)^2 dx'dy'$$

$$- \iint_D \left(\frac{\partial \mathcal{E}}{\partial y'}\right)^2 dx'dy' \qquad (2.52)$$

Now each of these integrals can be expressed in a quadric form, so that if I is expressed as $U^T A U$, then matrix A can be expressed as the sum of three matrices.

$$A = A_1 - \frac{1}{r^2} A_2 - A_3 \qquad (2.53)$$

Since $(1/r^2)$ appears as a scalar which multiplies A_2, no reformulation of matrices A_1, A_2, A_3 is needed when the aspect ratio r is changed. This permits the method to consider arbitrary changes in aspect ratios without any additional reformulation. As a result, the aspect ratio can be read as an input datum by the algorithm.

The steps involved in the algorithm are given as follows.

1. Read the values of V number, aspect ratio r, and an estimate of b.
2. Read the index profile $f(x',y')$ at grid points.
3. Set-up matrices A and B.
4. Calculate B^{-1} A.

5. Apply the power method to find λ, the eigenvalue and U, the eigenvector of $B^{-1} A$.
6. Calculate b.
7. Print the values of $E(x',y')$ at the grid points (the field profile) and the value of b (the normalized propagation constant).

2.4.4 Verification and Case Studies

The algorithm is coded in FORTRAN. The main program reads the index, sets up the A and B matrices and calls separate subroutines for matrix inversion and eigenvalue estimation. Double precision arithmetic is used to keep the numerical errors in the matrix inversion as small as possible.

To verify the accuracy of our Variational-Finite difference method, a specific asymmetrical step index channel waveguide ($n_{channel} = 1.05 \times n_{substrate}$) is considered. For this waveguide, the b-V characteristics have already been calculated by Marcatili [Ma69]. Figures 2.19 and 2.20 show the results for the aspect ratios 1 and 2 respectively. It is seen that results are in excellent agreement, establishing the validity of the Variational-Finite difference method. The results of the Variational-Finite difference method, however, are useful for any arbitrary aspect ratio and index profile.

The cases of practical importance are diffused channel waveguides with index profiles functions mentioned below.

$$f(x',y') = e^{-x'^2} \cdot e^{-y^2} \tag{2.54}$$

$$f(x',y') = \mathrm{erfc}(x') \cdot e^{-y'^2} \tag{2.55}$$

The profile in equation (2.54) is called the Gaussian-Gaussian index profile which results from a diffusion process in which the dopant source is depleted entirely during diffusion. This condition is valid for indiffusion of Titanium in $LiNbO_3$. For glass waveguide fabrication, the diffusion is essentially from an infinite source of silver ions in the salt bath. For this case, the profile can be approximated as an erfc-Gaussian function (equation (2.55)). For these two profiles of practical importance, the b-V characteristics for the fundamental modes are computed. Figures 2.21 and 2.22 show the b-V characteristics for aspect ratios 1 and 2 respectively. In both the figures it is seen that for the same V number, the step index waveguide has the highest b followed by the Gaussian-Gaussian and erfc-Gaussian waveguides. A similar trend is observed in the planar graded index waveguides as illustrated in figure 2.5.

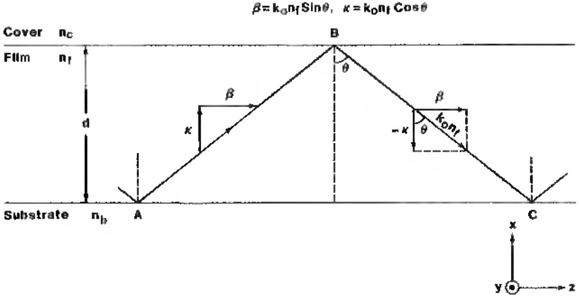
$\beta = k_0 n_f \sin\theta, \quad \kappa = k_0 n_f \cos\theta$
Cover n_c
Film n_f
Substrate n_b
d
A
B
C
κ
β
θ
$-\kappa$
$k_0 n_f$
x
y
z

Figure 2.1 Ray diagram for the step index waveguide

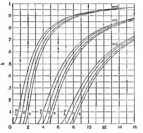

Figure 2.2 b-V characteristics for the step index waveguide

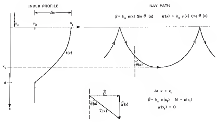
INDEX PROFILE
Δn
n_c
n_b
n_s
f(x)
x_t
d
x
RAY PATH
$\beta = k_o\, n(x) \sin\theta\,(x)$ $\kappa(x) = k_o\, n(x) \cos\theta\,(x)$
θ(x)
$\vec{\beta}$
θ(x)
$\vec{k}(x)$
$\vec{\kappa}(x)$
At $x = x_t$
$\beta = k_o\, n(x_t)$ $N = n(x_t)$
$\kappa(x_t) = 0$

Figure 2.3 Ray diagram for the graded index waveguide

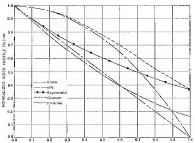

Figure 2.4 Normalized index profile functions

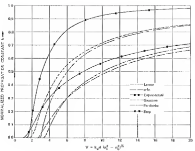

Figure 2.5 b-V characteristic for m=0 for various index profiles

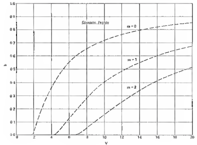

Figure 2.6 b-V characteristics for m=0,1,2 for Gaussian profile

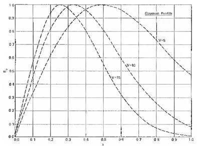

Figure 2.7 Field profiles for m=0, V=5,10,15 for Gaussian profile

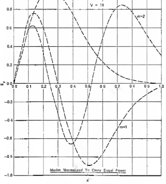

Figure 2.8 Field profiles for m=0,1,2, for Gaussian profile

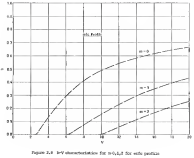

Figure 2.9 b-V characteristics for m=0,1,2 for erfc profile

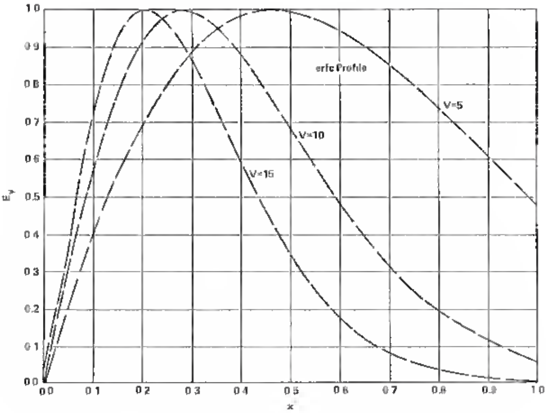

Figure 2.10 Field profiles for m=0, V=5,10,15 for erfc profile

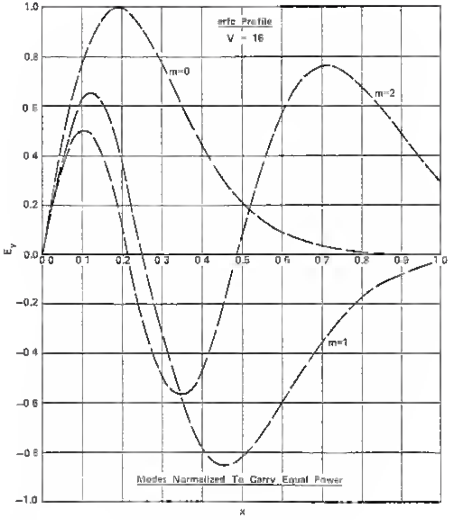

Figure 2.11 Field profiles for m=0,1,2 for erfc profile

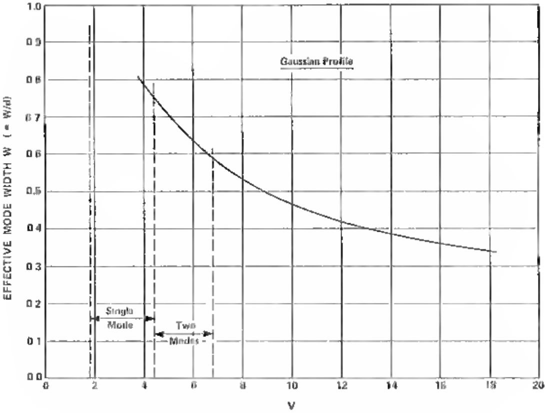

Figure 2.12 Effective normalized modal width for m=0 for Gaussian profile

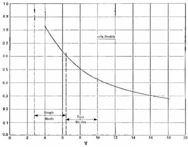

Figure 2.13 Effective normalized modal width for m=0 for erfc profile

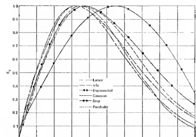

Figure 2.14 Comparison of the field profile for m=0 for various index profiles

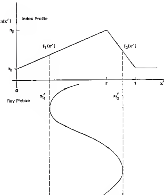
$n(x')$
Index Profile
n_p
n_b
$f_1(x')$
$f_2(x')$
0
r
1
x'
Ray Picture
x'_{t_1}
x'_{t_2}

Figure 2.15 Ray diagram for the buried waveguide

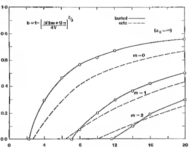

Figure 2.16 b-V characteristics for the buried waveguide

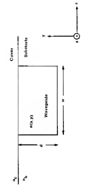
Cover
Substrate
n_c
n_b
$n(x,y)$
Waveguide
d
w
x
y
z

Figure 2.17 Channel waveguide geometry

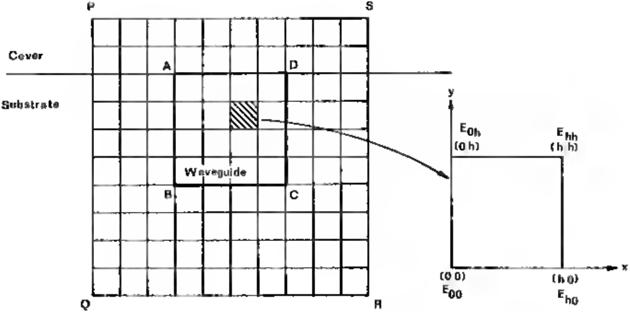
P
S
Cover
Substrate
A
D
B
C
Waveguide
Q
R
y
x
E0h
(0 h)
Ehh
(h h)
(0 0)
E00
(h 0)
Eh0

Figure 2.18 Rectangular grid for the Variational-Finite difference method

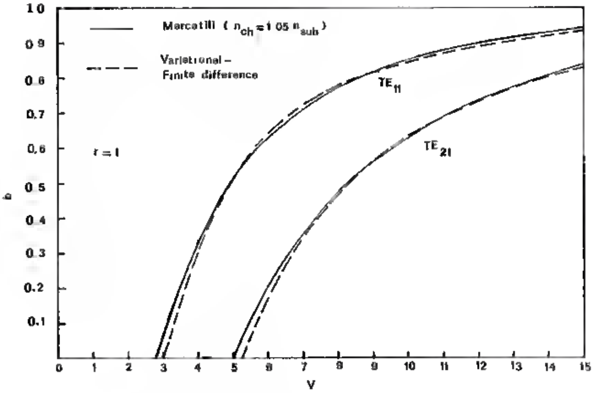

Figure 2.19 b-V characteristics for the step index channel waveguide with $r=1$

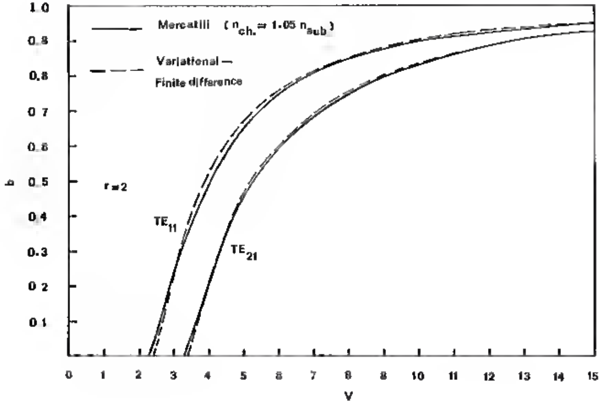

Figure 2.10 b-V characteristics for the step index channel waveguide with r=2

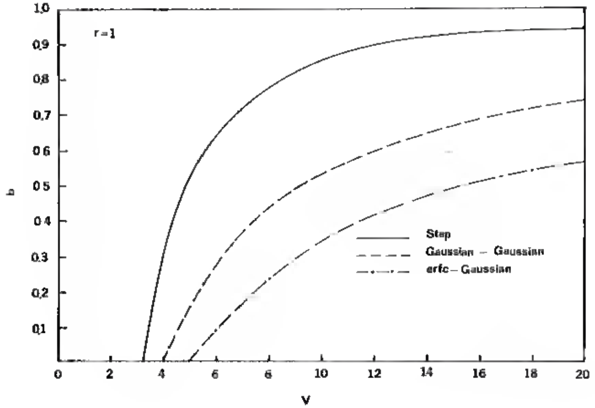

Figure 2.21 b-V characteristics, m=0,r=1 for channel waveguides with various index profiles

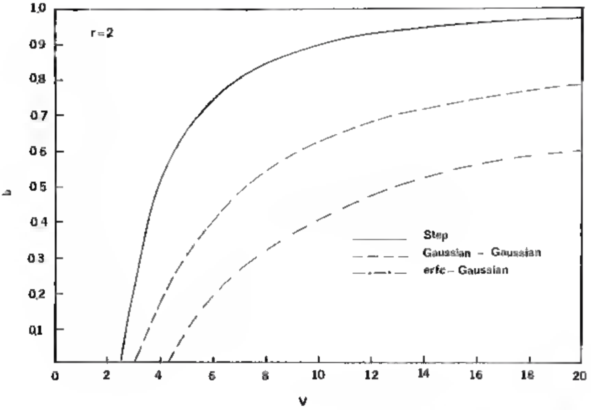

Figure 2.22 b-V characteristics, m=0, r=2 for channel waveguides with various index profiles

CHAPTER THREE
DIFFUSION SIMULATION

The study of ion-exchange/diffusion in glass is important because this phenomenon controls the formation of waveguides on the surface of glass. The diffusion mechanism essentially determines the device parameters such as the guide depth and the index profile while ion-exchange controls the magnitude of the index change at the surface. When an ordinary soda-lime-silicate glass slide is placed in a molten salt bath containing monovalent ions such as Ag^+, K^+, Li^+ or Tl^+, these ions exchange with the sodium ions (Na^+) in glass at the phase boundary between the glass and the melt and then migrate inside the glass by a process of diffusion. The general problem of diffusion of ions in glass has been studied in great detail by Doremus [Do64]. He has modelled the transport of silver ions in glass as an "inter-diffusion process" involving silver and sodium ions. The equations describing the inter-diffusion process are derived as follows.

Consider two monovalent ion species A and B which are undergoing inter-diffusion in glass. Let ϕ_A and ϕ_B be their fluxes and D_A and D_B be their self-diffusion coefficients.

From the Nernst-Plank equation [He58] the flux ϕ_A can be expressed as

$$\phi_A = -D_A \nabla C_A + D_A C_A (\frac{RT}{F}) E \qquad (3.1)$$

where

C_A = Concentration of A

R = Gas constant, 8.317 J/K-mole

F = Faraday Constant, 96500 J/V-mole

T = Absolute temperature, °K

E = Electric Field, V/mm

The electric field may be applied externally or may be present as a gradient of the diffusion potential.

The similar equation can be written for ϕ_B

$$\phi_B = -D_B \nabla C_B + D_B C_B (\frac{RT}{F}) E \qquad (3.2)$$

Electroneutrality requires that the total concentration of the two ion species be constant, so that

$$C_A + C_B = C \qquad (3.3)$$

Moreover, there is no net current, i.e.,

$$\phi_A + \phi_B = 0 \tag{3.4}$$

Taking the gradient of equation (3.3),

$$\nabla C_A + \nabla C_B = 0 \tag{3.5}$$

$$\nabla C_A = -\nabla C_B \tag{3.6}$$

Substituting equations (3.4) and (3.6) in equations (3.1) and (3.2), an expression for ϕ_A can be derived as

$$\phi_A = -\left(\frac{D_A\ D_B(C_A + C_B)}{D_A\ C_A + D_B\ C_B}\right) \nabla C_A \tag{3.7}$$

Thus, one can define an inter-diffusion coefficient D_{AB} as

$$D_{AB} = \frac{D_A\ D_B(C_A + C_B)}{D_A\ C_A + D_B\ C_B} \tag{3.8}$$

Then,

$$\phi_A = -D_{AB}\ \nabla C_A \tag{3.9}$$

$$\phi_B = -D_{AB}\ \nabla C_B \tag{3.10}$$

It is clear from equation (3.8) that the inter-diffusion coefficient D_{AB} is concentration dependent. During the fabrication of glass waveguides using silver-sodium ion-exchange, the concentration of silver ions in the bath (and hence, in the waveguide) is much smaller than that of the sodium ions. This fact considerably simplifies the diffusion equation as follows.

If we assume

D_A = self-diffusion coefficient of Ag^+

C_A = concentration of Ag^+

D_B = self-diffusion coefficient of Na^+

C_B = concentration of Na^+

As mentioned above, $C_A << C_B$, with the result, equation (3.8) simplifies as

$$D_{AB} = D_A \tag{3.11}$$

Thus, the silver self-diffusion has a stronger influence on the inter-diffusion process and D_{AB}, which in general is concentration dependent, can be assumed to be constant in this case.

With this simplification, several cases arising in practical fabrication are considered in detail in the following sections.

3.1 One-Dimensional Diffusion Without Drift Field

When a glass slide is placed in a molten salt bath (T = 330°C) for diffusion, the Ag^+/Na^+ ion-exchange takes place entirely on its surface with the ions penetrating to the depth of about 6-10 µms in about 60-80 minutes. The diffusion can thus be considered one-dimensional. The number of ions entering the glass slide is much smaller than those present in the salt bath, so that the concentration c_0 of silver ions in the melt can be assumed to be constant over the entire period of diffusion.

The one-dimensional diffusion equation with constant diffusion coefficient is [Cr56]

$$\frac{\partial c}{\partial t} = D \frac{\partial^2 c}{\partial x^2} \tag{3.12}$$

With the initial condition, $c(x,0) = 0$ for $x > 0$ and the boundary condition $c(0,t) = c_0$.

The method of Laplace transforms is used to get a closed form solution of this equation for the above mentioned boundary and initial conditions.

Consider the function $c(x,t)$ and define its Laplace transform $\overline{C}$ as

$$\overline{C} = \int_0^\infty e^{-st} c(x, t) \, dt \tag{3.13}$$

Multiplying both sides of equation (3.12) by e^{-st} and integrating with respect to t from 0 to ∞,

$$\int_0^\infty e^{-st} \frac{\partial^2 c}{\partial x^2} dt - \frac{1}{D} \int_0^\infty e^{-st} \frac{\partial c}{\partial t} dt = 0 \qquad (3.14)$$

It can be assumed that for a well behaved function c(x,t), the orders of differentiation and integration in equation (3.14) can be interchanged. Therefore, for the first term in equation (3.14),

$$\int_0^\infty e^{-st} \frac{\partial^2 c}{\partial x^2} dt = \frac{\partial^2}{\partial x^2} \int_0^\infty c\, e^{-st} dt = \frac{\partial^2 \overline{C}}{\partial x^2} \qquad (3.15)$$

Also, integrating by parts,

$$\int_0^\infty e^{-st} \frac{\partial c}{\partial t} dt = [e^{-st} c] \Big|_0^\infty + s \int_0^\infty c\, e^{-st} dt = s\overline{C} \qquad (3.16)$$

The term in the square bracket vanishes at t = 0 by virtue of the initial condition and at $t = \infty$ by the exponential factor. Thus, equation (3.12) reduces to

$$D \frac{\partial^2 \overline{C}}{\partial x^2} = s\overline{C} \qquad (3.17)$$

The boundary condition $c(0,t) = c_0$ can be transformed as

$$\overline{C}(0) = \int_0^\infty c(0,t)\, e^{-st} dt = \int_0^\infty c_0\, e^{-st} dt = \frac{c_0}{s} \qquad (3.18)$$

The ordinary differential equation (3.17) with the boundary condition, equation (3.18) has a solution which remains finite when $x \to \infty$ is given by

$$\overline{C}(s) = \frac{c_0}{s} e^{-x\sqrt{s/D}} \tag{3.19}$$

The inverse transform of $\overline{C}(s)$ is given by

$$c(x,t) = c_0 \operatorname{erfc}\left(\frac{x}{2\sqrt{Dt}}\right) \tag{3.20}$$

where

$$\operatorname{erfc}(z) \triangleq 1 - \frac{2}{\sqrt{\pi}} \int_0^z e^{-p^2}\, dp \tag{3.21}$$

3.2 One-Dimensional Diffusion With Drift Field

Application of an electric field can considerably enhance the diffusion process during the fabrication of glass waveguides. This is achieved by depositing a metal electrode on the back surface of the glass slide and applying a voltage between the electrode and the melt to set-up an electric field inside the glass slide. For this case, the diffusion equation (3.12) is modified by including an extra term corresponding to the E field as

$$\frac{\partial c}{\partial t} = D \frac{\partial^2 c}{\partial x^2} - E\mu \frac{\partial c}{\partial x} \tag{3.22}$$

where

E = externally applied electric field

μ = mobility of silver ions in glass

It should be noted that both the diffusion coefficient and mobility vary with temperature and the temperature dependence is given by an Arhenius type relation [Do64]

$$D = D_0 \, e^{-\Delta H/RT} \tag{3.23}$$

$$\mu = \mu_0 \, e^{-\Delta H/RT} \tag{3.24}$$

where ΔH is the activation energy.

To tailor the index profile, usually the electric field E is changed with time. Under this condition, no closed form solution for equation (3.22) is available and one has to resort to numerical techniques. A number of methods have been devised whereby some or all of the partial derivatives in euqation (3.22) are replaced by finite-difference approximations. A rectangular region is defined in the t-x domain with t as the ordinate and x as the abscissa as shown in figure 3.1. Line PS represents the condition $x = 0$, so the boundary condition $c(0,t)$ is used to assign the values of concentration at grid points on the line PS. Line PQ represents the condition $t = 0$, so the initial condition $c(x,0)$ is used to assign the value of concentration on the line PQ.

Inside the region PQRS, discrete variables i and j are associated with x and t, respectively. The partial derivatives at point (i,j) are then approximated as

$$\frac{\partial^2 c}{\partial x^2} = \frac{c(i+1,j) - 2c(i,j) + c(i-i,j)}{(\Delta x)^2} \tag{3.25}$$

$$\frac{\partial c}{\partial x} = \frac{c(i+i,j) - c(i-i,j)}{2\Delta x} \tag{3.26}$$

$$\frac{\partial c}{\partial t} = \frac{c(i,j) - c(i,j-i)}{\Delta t} \tag{3.27}$$

Then the partial differential equation (3.22) is transformed into a set of coupled difference equations by using the approximations (3.25) through (3.27).

$$\frac{c(i,j) - c(i,j-i)}{\Delta t} = D\left[\frac{c(i+1,j) - 2c(i,j) + c(i-1,j)}{(\Delta x)^2}\right] \tag{3.28}$$

$$- E(j)\ \mu\left[\frac{c(i+1,j) - c(i-1,j)}{2\Delta x}\right]$$

Define

$$\frac{D\Delta t}{(\Delta x)^2} = a \tag{3.29}$$

and

$$\frac{E(j)\ \mu\ \Delta t}{2\Delta x} = \beta(j) \tag{3.30}$$

Then,

$$c(i,j) - c(i,j-1) = ac(i+1,j) - 2ac(i,j) + ac(i-1,j) \tag{3.31}$$

$$- \beta(j)\ c(i+1,j) + \beta(j)\ c(i-1,j)$$

$\therefore$

$$c(i,j) = \frac{[(a - \beta(j))c(i+1,j) + (a + \beta(j))\ c(i-1,j)]}{(1 + 2a)} \tag{3.32}$$

$$+ c(i,j-1)$$

The simulation starts at line PO where the values of the concentration are known and proceeds along the time axis, each time taking the next horizontal line and iterating along the line till convergence is reached (figure 3.1).

The algorithm is coded in FORTRAN and a special graphics software package is developed to plot the concentration profiles for various times. This package consists of graphics subroutines written in FORTRAN to plot curves and surfaces. To test the program, the electric field is set to zero so that the field assisted diffusion equation (3.22) reduces to the standard diffusion equation (3.12) for which a closed form analytical solution is available. The concentration profiles for t = 10 to 50 minutes are shown in figure 3.2. This numerical solution shows an excellent agreement with the analytical solution (complementary error function) establishing the validity of the algorithm.

The program is then used to calculate the concentration profile resulting from different values of E in the range of 0-100 volts/mm and t in the range of 10-50 minutes. These ranges are chosen considering the actual values of E and t used in our experiments. Figures 3.3 and 3.4 show the results corresponding to various process conditions. It can be seen that the effects of time and field are interchangeable, i.e., one can choose a small value of field for large time or a large value of field for small time to get approximately the same concentration profile. To be specific, in figures 3.3 and 3.4, waveguides with E = 60 v/mm and t = 30 minutes have approximately the same profile as those with E = 40 v/mm and t = 50 minutes.

Figure 3.5 illustrates how the field can be used to tailor the index profile. For small values of time, i.e., t = 10 minutes, the profile resembles a complementary error function. As time proceeds, the profile changes to the

Gaussian-like shape and subsequently to almost the step index profile. Thus, the simulation has shown that a judicious combination of E and t can be used to get any profile between erfc to Gaussian to step. For a step-like profile, however, a large value of field should be used for a large diffusion time.

3.3 Two-Dimensional Diffusion With And Without Drift Field

In the previous section, one-dimensional diffusion simulation suitable for planar waveguide application has been considered. Channel waveguides in glass require diffusion through a window which requires analysis of two-dimensional diffusion. The diffusion equation for the two-dimensional diffusion with drift field is

$$\frac{\partial c}{\partial t} = D \nabla^2 c - \mu \vec{E} \cdot \vec{\nabla} c \tag{3.33}$$

The thickness of the glass substrate is approximately 1 mm and the region near the top surface where the diffusion takes place is approximately 10-15 µm deep. Thus, the field in that region can be assumed to be perpendicular to the glass surface which is the y direction. Thus,

$$\vec{E} \cdot \vec{\nabla} c = E \frac{\partial c}{\partial y} \tag{3.34}$$

with this simplification,

$$\frac{\partial c}{\partial t} = D\frac{\partial^2 c}{\partial x^2} + D\frac{\partial^2 c}{\partial y^2} - \mu E\frac{\partial c}{\partial y} \tag{3.35}$$

The concentration c in this case is a function of three independent varibles, i.e., $c = c(x,y,t)$.

In the numerical solution of equation (3.35) a three-dimensional array $c(i,j,k)$ is defined where discrete variables i, j, k are associated with variables x, y, t respectively,

The following approximations are made for the partial derivatives:

$$\frac{\partial c}{\partial t} = \frac{c(i,j,k) - c(i,j,k-1)}{\Delta t} \tag{3.36}$$

$$\frac{\partial^2 c}{\partial x^2} = \frac{c(i+1,j,k) - 2c(i,j,k) + c(i-1,j,k)}{(\Delta x)^2} \tag{3.37}$$

$$\frac{\partial^2 c}{\partial y^2} = \frac{c(i,j+1,k) - 2c(i,j,k) + c(k,j-1,k)}{(\Delta y)^2} \tag{3.38}$$

$$\frac{\partial c}{\partial y} = \frac{c(i,j+1,k) - c(i,j-1,k)}{2(\Delta y)} \tag{3.39}$$

The same method as outlined in the previous section is used to solve the difference equation approximation of the partial differential equation (3.35). Simulation is carried out for different window sizes w, electric field E and time t and the results are shown in figures 3.6-3.13. The following observations are in order:

1. The window size has a rather small effect on the effective depth of the waveguide for both ordinary and field assisted diffusions. In figures 3.6 and 3.7, the applied field is zero and for both window sizes w = 5 and w = 10 µm, the effective depth is approximately 5 µm for t = 50 minutes. However, as seen in figures 3.8 and 3.9 with an applied field of 30 v/mm for both cases, the depth has increased to ≈ 10 µm for the same t = 50 minutes.
2. For waveguides fabricated without an applied field, the sideways diffusion seems to dominate, making them quite shallow. Their aspect ratio, which is the ratio of the waveguide effective width to its effective depth, is also ≈ 2 or more. For example in figure 3.6, effective width ≈ 18 µm and effective depth = 5 µm, so aspect ratio = 3.6. In figure 3.7, effective width = 10 µm, effective depth = 5 µm, so aspect ratio ≈ 2.
3. With field assisted diffusion, considerable penetration of silver ions without sideways diffusion is achieved resulting in almost square waveguides. In figure 3.9, w = 5 µm, E = 30 v/mm, t = 50 min., effective width ≈ 10 µm, effective depth ≈ 8 µm. This waveguide is likely to have good coupling with an optical fiber with core diameter of 10 µm.

These results indicate that this program can be effectively used to design channel waveguides exhibiting good coupling efficiencies with optical fibers of specified core diameters. In other words, the values of mask width w, E field and the time of diffusion t can be chosen so that the resultant waveguide has approximately the same effective depth and width as that of the fiber. Figures 3.10–3.13 illustrate the concentration surfaces for the above-mentioned cases. While running the program for different values of w, E and t, these figures are displayed on the CRT terminal. The visual information conveyed by them is then used to determine the effect of changing the value of w, E and t on the shape and size of the concentration surface, thus facilitating faster design procedures.

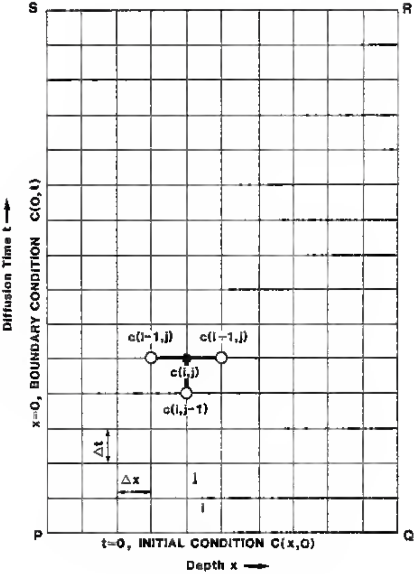
S
R
Diffusion Time t →
x=0, BOUNDARY CONDITION C(O,t)
c(i-1,j)
c(i+1,j)
c(i,j)
c(i,j-1)
Δt
Δx
j
i
P
Q
t=0, INITIAL CONDITION C(x,O)
Depth x →

Figure 3.1 Rectangular grid for one dimensional diffusion simulation

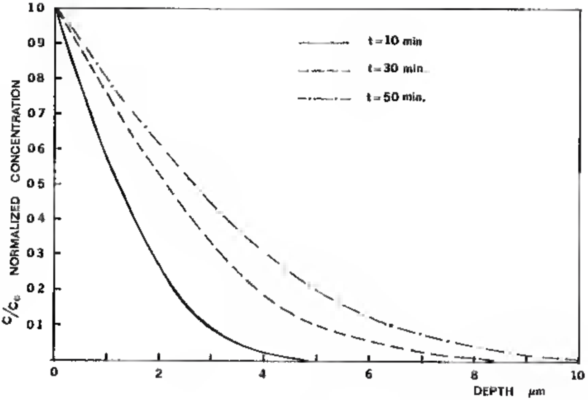

Figure 3.2 Concentration profiles for one dimensional diffusion without applied field

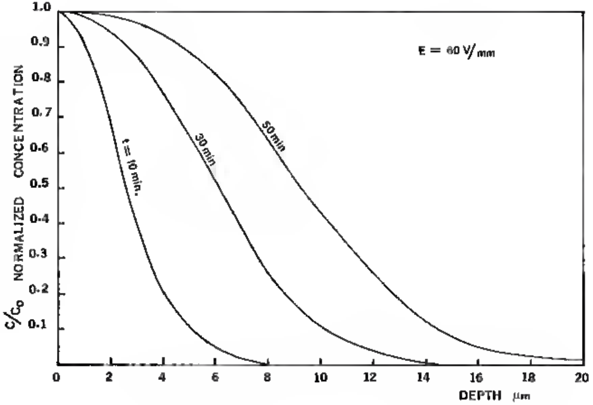

Figure 3.3 Concentration profiles for field assisted diffusion for various diffusion times

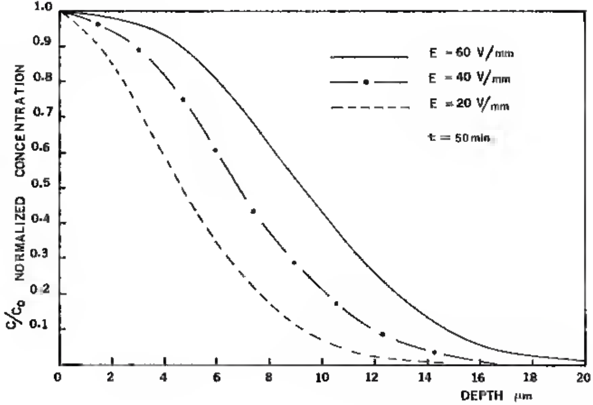

Figure 3.4 Concentration profiles for field assisted diffusion for various values of the applied field

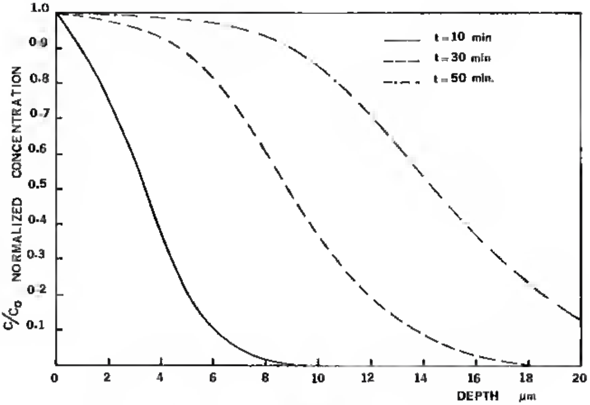

Figure 3.5 Tailoring of the index profile by an applied electric field

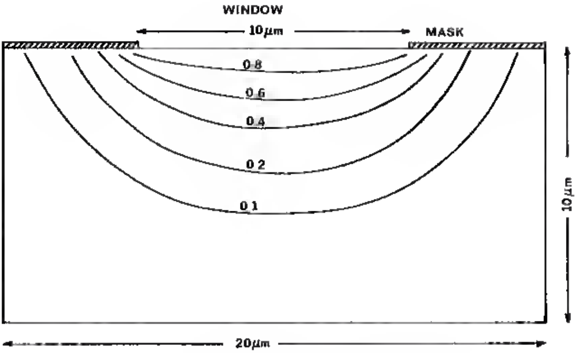

Figure 3.6 Concentration contours for E=0 V/mm, t=50 min , w=10 microns

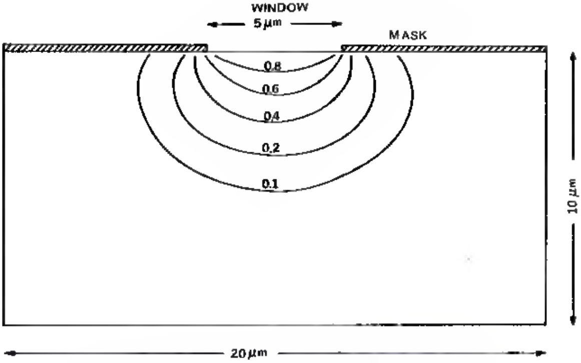

Figure 3.7 Concentration contours for E=0 V/mm, t=50 min , w=5 microns

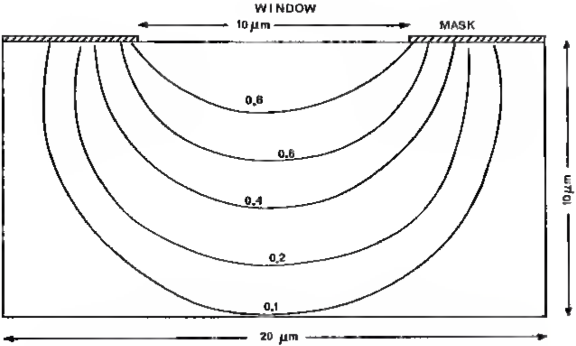

Figure 3.8 Concentration contours for E=30 V/mm, t=50 min., w=10 microns

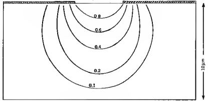
WINDOW
5μm
MASK
0.8
0.6
0.4
0.2
0.1
10μm
20μm

Figure 3.9 Concentration contours for E=30 V/mm, t=50 min., w=5 microns

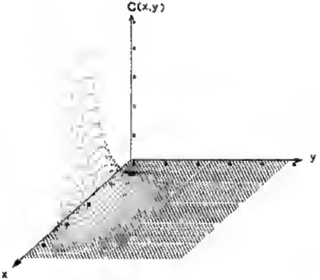

Figure 3.10   Concentration surface for E=0 V/mm, t=50 min., w=5 microns

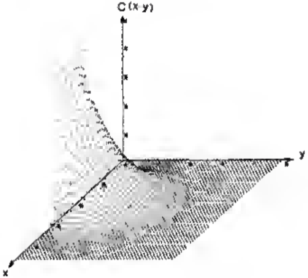

Figure 3.11 Concentration surface for E=30 V/mm, t=50 min., w=5 microns

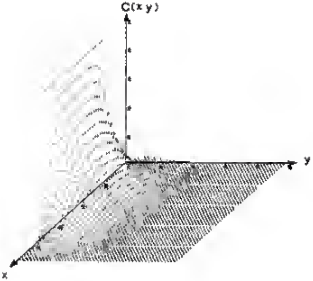

Figure 3.12 Concentration surface for E=0 V/mm, t=50 min., w=10 microns

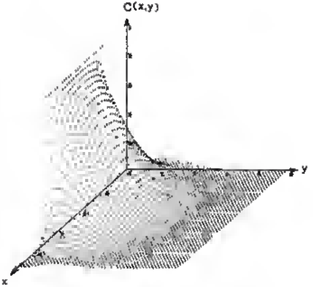

Figure 3.13 Concentration surface for E=30 V/mm, t=50 min., w=10 microns

CHAPTER FOUR
WAVEGUIDE FABRICATION

4.1 Fabrication Process

The process used for fabricating ion-exchanged glass waveguides as reported in literature [Iz72, St77, Ch80] is shown in figure 4.1. It has a salt bath containing a mixture of approximately 90% (by weight) sodium nitrate ($NaNO_3$) and 10% silver nitrate ($AgNO_3$) heated to a temperature of 320-360°C. A soda-lime-silicate glass substrate, about 1 mm thick, is suspended in the bath for a period of 40-60 minutes. The silver ions (Ag^+) in the bath replace the sodium ions (Na^+) in the glass slide, thus forming a thin waveguide at the surface. As Ag^+ has higher polarizability compared to Na^+, the surface region doped with Ag^+ exhibits higher refractive index, enabling light guidance. A variation of this process is shown in figure 4.2 in which a metallic electrode is deposited on the back surface of the glass slide to facilitate the application of an electric field which enhances the diffusion of silver ions. Standard photolithographic masking and delineation are used to form a window or strip pattern using aluminum mask as shown in figure 4.2. Ion-exchange through the strip region is used to fabricate channel waveguides.

In spite of several sporadic attempts spread over about 10 years (1972–1982), no one has fabricated low-loss single mode waveguides with assured reproducibility. As a result, these attempts have been mainly research oriented and so far the results have not been encouraging from a practical standpoint. The results of diffusion simulation and propagation analysis performed as a part of this project indicate that the silver ion concentration in the bath is an important parameter which needs to be monitored and controlled in order to make reproducible waveguides. This is especially true for multimode waveguides and batch processing of single mode waveguides. In this context, the following observations concerning the existing process are in order:

1. Process parameters such as temperature and time of diffusion are controlled accurately (temperature within ±0.5°C).
2. The existing process takes high weight ratio of $AgNO_3$ to $NaNO_3$ resulting in multimode (7–16 modes) waveguides.
3. With such a high concentration, reduction of silver ions to the metallic state is highly likely which can cause excessive absorption and scattering loss.
4. The time of diffusion necessary to produce a single mode waveguide with such heavy concentration of silver ions is only about 2–3 minutes. This makes the timing very critical, thus making the reproducibility a serious problem.

5. A single mode waveguide fabricated under such conditions is usually shallow. Therefore, such a guide couples poorly to an optical fiber which can be thought of as a buried structure of reasonably large cross-sectional dimension (8–10 μm).
6. No concentration control has every been attempted.

In order to overcome these problems, it was thought necessary to start out with very small concentration of silver ions and then control it precisely at all times during diffusion. The reduction of Ag^+ concentration would allow the time of diffusion to increase to the order of 40–60 minutes even for a single mode waveguides, thus eliminating the time control problem.

A novel process capable of releasing precise amount of silver ions was developed to solve these problems [Le84b]. The idea is based on the well known Faraday's law of electrolysis:

When 96500 coulombs of charge are passed through a metallic electrode, 1 gram equivalent of the metal is released into the solution as ions.

Thus, generation for silver ions can be accomplished by using a metallic silver electrode rather than a salt mixture of $AgNO_3$ and $NaNO_3$. Furthermore, melt impurities can be kept minimal as ultra pure (99.999%) silver rods are commercially available. The process of releasing silver ions can now be electronically controlled through the realization of an accurate variable current source using off-the-shelf operational amplifiers. In addition, the Ag^+ concentration in the bath can be changed with time so that the diffusion can be carried out with a variety of boundary conditions, thus providing a larger control of the refractive index profile. The basic schematic diagram of the electrolytic process is shown in figure 4.3. The set-up consists of a salt bath heated by a band heater coiled around it. The temperature of the bath is sensed by a thermocouple and controlled with a closed-loop controller to an accuracy of ±0.5°C. The current source is essentially a voltage to current converter, where a Zener stabilized input voltage produces precise output current with an accuracy of ±0.1 mA. The redox (reduction-oxidation) reactions at the electrodes are

Anode (silver rod)

$$Ag_{(metal)} \rightarrow Ag^+ + \overline{e}$$

Cathode (platinum wire)

$$Ag^+ + \overline{e} \rightarrow Ag_{(metal)}$$

$$Na^+ + \overline{e} \rightarrow Na_{(metal)}$$

Since sodium is more reactive than silver, it has more propensity to stay in ionic form and thus, it is less likely to be deposited as sodium metal. To prevent the released silver ions from depositing back as metallic silver, a fritted glass enclosure is used around the platinum wire as shown in figure 4.4. The bore size in the fritted glass is ≈ 2-4 µm. It essentially prevents the silver ions to reach the platinum wire by convection so that only the sodium ions are made to react at the cathode producing metallic sodium which collects inside the fritted glass enclosure [Na84]. The rate at which silver ions diffuse through the bores in the frit is much smaller than that at which they are generated by electrolysis, so that a very good control on the release of silver ions is achieved. This novel technique has an inherent ability to generate precise, low-level silver ion concentration. This capability is extensively used in this project work to facilitate fabrication of reproducible single mode waveguides.

4.2 Concentration Measurement

The electrolytic process which can generate precise number of silver ions must be complemented by a measurement technique which can monitor the silver ion concentration on-line. The conventional methods to measure concentration, e.g., mass spectrometry, atomic absorption, emission and fluorescent spectrometry and nuclear activation are not suitable as they are off-line, thus, cannot be used in the feedback control. Commercially available electrodes which are sensitive for selective ions, unfortunately, operate at relatively low temperature (0-80°C) and therefore are useful only for aqueous solutions. A special transducer which can be used in a molten salt environment (high temperatures in the range of 300-400°C) and can measure ion concentration *in situ* has been developed [La84c]. The operation of the transducer is described in the remainder of this section.

As shown in figure 4.5, the glass bulb transducer is basically a galvanic cell in which the redox reaction is used to generate a cell potential. This potential depends upon the substances that make up the cell and their concentration. Since in this particular cell the same substance is present in both the anode and cathode compartments, the cell potential is a measure of the ionic concentrations in the cell.

The generated cell potential, called the Nernst potential, is given by [Bl59]

$$V = - 2.303 \frac{RT}{F} \log \left(\frac{c_1}{c_2}\right) \qquad (4.1)$$

where

R = gas constant (8.317 J/K-mole)

T = temperature in °Kelvin

F = Faraday constant (96500 J/V-mole $\overline{e}$)

c_1 = reference ionic concentration

c_2 = concentration to be measured

With these value of R and F substituted, equation (4.1) can be rewritten as

$$V = 1.98 \times 10^{-4}\ T \log \left(\frac{c_1}{c_2}\right) \tag{4.2}$$

Concentration cells using fritted glass [Du61] in place of glass bulb or glass tubes with asbestos fibers [Fl56] have been reported. It is our experience, however, that with fritted glass, complete mixing between the solutions occurs within an hour and the cell potential monotonically decreases, making the measurements unreliable. Fortunately with the glass cell, the glass bulb itself can be used as a good conducting membrane. Inman [In62] has reported the use of such a glass bulb containing reference electrode to form a part of the concentration cell. The underlying idea is that Pyrex glass at elevated temperature (330°C-370°C) can act as a resistive ion-bridge between the solutions since the sodium ions have rather high mobility at these temperatures. At there are no pores present within the membrane, the two solutions are physically isolated.

To fabricate the cell, a Pyrex glass test tube about 8 mm internal diameter with approximately 0.5 mm wall thickness is heated with a torch and blown at one end to form a glass bulb with a tubular stem. The glass bulb is nearly spherical in shape with about 12 mm diameter and about 0.1 mm wall thickness as shown in figure 4.6. A reference melt is produced by releasing 2.0 gms of silver from a high purity (99.999%) rod into a melt of 400 gms $NaNO_3$ by electrolysis. The reference melt concentration c_1 is approximately equal to 3.94×10^{-3} mole fraction (MF). The glass bulb is then filled to its neck with about 3 to 4 gms of the reference melt. High purity silver wires are also used as the cathode within the glass bulb as well as the anode immersed in the bath. The cell is then used to measure the silver ion concentration in the salt bath. The Nernst potential difference is measured with a 10 MΩ input impedance digital voltmeter.

By electrolytically releasing known quantities of Ag^+ ions in 400 gms of $NaNO_3$, different known concentrations of Ag^+ in $NaNO_3$ are prepared. By measuring the cell potential each time, a plot of cell emf vs. $\log(c_1/c_2)$, as shown in figure 4.7 is obtained. The solid line represents the theoretical cell potential as given by equation (4.2). As expected, both curves exhibit linear behavior. Both the experimental and theoretical lines have nearly the same slope, with the slope of the experimental line slightly lower. The temperature gradient in the bath in vertical direction amounts to almost 20°C. The bath temperature is 340°C and it is assumed to be the same in the reference melt. However, some temperature gradient is likely to exist between the contents of the glass bulb and that of the bath, causing the difference in the slope of the experimental and the theoretical line. Moreover, when two concentrations are equal, an asymmetry potential of about 14 mV is measured which is not predicted by equation (4.1). Although Inman [In62] attributes the asymmetry potential to a difference of sodium ion concentration in the glass between the inside and outside of the bulb which occurs during blowing, we believe the temperature difference causes this asymmetry potential [La84c].

With the development of the concentration transducer, it is possible to implement on-line concentration control. The equation (4.2) has a log term in it, so that an anti-log amplifier is needed to get a signal which varies linearly with Ag^+ ion concentration in the bath. In the feedback configuration, the Ag^+ concentetion can be monitored and when it falls below the preset value, additional silver ions can be released by periodically pumping currrent in the silver rod. The detailed schematic diagram of the entire process with all its instrumentation and controls, some already in place, is shown in figure 4.8. The implementation of the entire process control will make it possible to fabricate glass waveguides reproducibly since all the process variables viz. T, t and C_0 will be controlled.

4.3 Planar Waveguide Fabrication Procedure

(A) Silver ion releasing

1. Clean the aluminum beaker: Rinse the beaker with hot de-ionized (DI) water. Remove the surface layer on the inside wall of the beaker by boiling dilute aluminum etch (16-1-1-2 etch): 16 parts phosphoric acid, 1 part acetic acid, 1 part nitric acid and 2 parts DI water) for 10 minutes. Rinse with DI water. Dry in the oven at 150°C for 5-6 hours (preferably overnight).
2. Melt preparation: Weight 400 gms of pure $NaNO_3$ (A.C.S-grade, Fisher) using handgloves. Take care not to introduce any dirt or grease into the salt. Heat the beaker to 330°C. Handling with gloves, weigh the silver rod and note its initial weight. Add pure $NaNO_3$ to the fritted glass tube and insert the platinum wire inside the tube. Suspend the silver rod and the fritted glass tube in the molten $NaNO_3$ and wait till thermal equilibrium is reached. By pumping current through the silver rod--platinum wire circuit, release the required amount of silver. One hundred milliamperes of current for 60 minutes releases 0.4 gms of silver in the bath. The current and or time can be appropriately changed to release any arbitrary amount of silver ions in the melt. During the ion release, no precipitation should be observed and the molten salt should be clear. If not, some silver is being deposited back to metallic

form and the possible fault is a crack in the fritted glass disk. After the time has elapsed, reduce the current to zero, remove the silver rod from the melt, rinse it with hot DI water and weigh it again. Compare the weight loss with the theoretically calculated weight loss.

(B) Diffusion

1. Clean the glass slides: Boil in trichloroethylene (TCE), acetone and methanol for 10 minutes each. Rinse in warm DI water and spin dry. Hardbake at 150°C for 60 minutes.
2. Place the slides inside the melt for the required time of diffusion.
3. Remove the slides from the bath after diffusion and let them cool for 10 minutes.
4. Remove the solidified salt on the slides (now waveguides) by shaking them in warm DI water. Wipe the waveguides with soft tissue paper.
5. Clean the waveguides surface with acetone. The waveguides are now ready for coupling light and measurement of the mode indices.

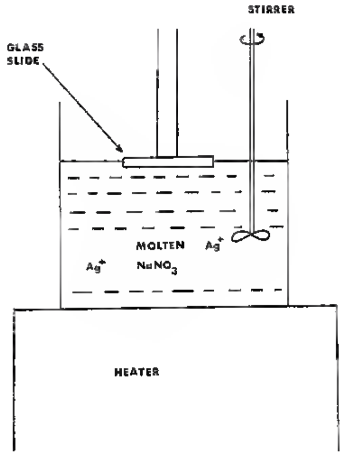
STIRRER
GLASS SLIDE
MOLTEN NaNO$_3$
Ag$^+$
Ag$^+$
HEATER

Figure 4.1 Existing process for glass waveguide fabrication

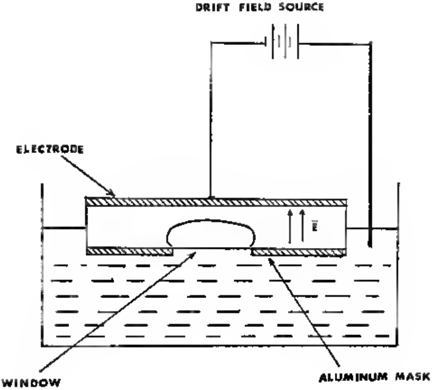
DRIFT FIELD SOURCE
ELECTRODE
E
WINDOW
ALUMINUM MASK

Figure 4 2   Process for field assisted diffusion of silver ions in glass

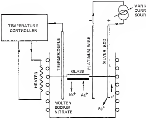
VARIABLE
CURRENT
SOURCE
TEMPERATURE
CONTROLLER
THERMOCOUPLE
PLATINUM WIRE
SILVER ROD
−
+
GLASS
HEATER
Na+
Ag+
e−
Ag+
MOLTEN
SODIUM
NITRATE

Figure 4.3 Electrolytic process for releasing silver ions

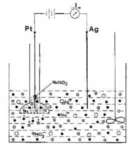
I
Pt
Ag
NaNO$_3$
Ag$^+$
Na$^+$
Na$^+$
NO$_3^-$

Figure 4.4 Introduction of fritted glass around cathode in the electrolytic process

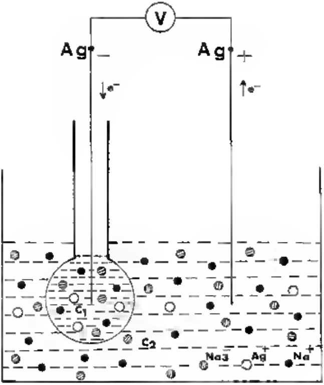
V
Ag −
Ag +
e⁻
e⁻
C1
C2
Na3
Ag+
Na+

Cathode

$Ag^+(C_1) + e^- \rightarrow Ag(s)$

Anode

$Ag(s) \rightarrow Ag^+(C_2) + e^-$

Figure 4.5 A concentration cell for measuring silver ion concentration

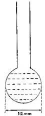

Figure 4.6 Glass bulb used in the reference electrode of the concentration cell

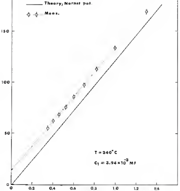

Figure 4.7 Measured and calculated Nernst potential for the concentration cell

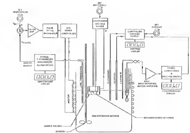
SP1 TEMPERATURE
ERROR AMP
PULSE WIDTH MODULATOR
SCR POWER CONTROLLER
CONTROLLED VOLTAGE SOURCE
CONTROLLED CURRENT SOURCE
SP3 CURRENT
000.0
CURRENT DISPLAY
ANALOG OUTPUT
DIGITAL THERMOMETER WITH ANALOG OUTPUT OPTION
000.0
TEMPERATURE DISPLAY
HEATER
HIGH INPUT IMPEDANCE BUFFER AMPLIFIER
DIGITAL CONDITIONER & MULTIVOLTMETER
000.0
CONCENTRATION DISPLAY
MOLTEN SODIUM NITRATE
SAMPLE HOLDER
STIRRER
SALT BATH

Figure 4.8 Detailed schematic diagram for the electrolytic process

CHAPTER FIVE
PLANAR WAVEGUIDE CHARACTERIZATION

5.1 Mode Index Measurement

One of the most useful techniques employed in the evaluation of the propagation constant of planar surface waveguides is the prism coupling technique. As shown in figure 5.1, a He-Ne laser beam is incident on a prism whose refractive index is higher than that of the film. The prism is placed on the surface of the guiding film so that the air gap between the film and the prism is small compared to the wavelength of the incident light. At specific angles, energy tunnels through the gap region and couples to the guiding mode. Thus, each guiding mode is characterized by a specific coupling angle and accurate measurement of these angles enables one to calculate N_m, the effective mode index of the m^{th} guided mode.

Figure 5.2 shows a ray picture of the prism coupler. Let

i = angle of incidence

α = angle of the prism

r = angle of refraction

n_p = prism refractive index

The travelling wave in the prism has a wave vector with magnitude $k_o n_p$ which can be decomposed into a horizontal component $k_o n_p \cos\theta$ and a vertical component $k_o n_p \sin\theta$. The tunneling interaction takes place when the horizontal component of the wave vector (along the z direction) is equal to the propagation constant of a given mode among the many possible modes of the waveguide. Under this condition that particular mode gets excited [Ti71].

Thus,

$$\beta = k_o n_p \cos\theta \tag{5.1}$$

However,

$$\beta = k_o N ,$$

so that $N = n_p \cos\theta$. (5.2)

Now in Δ ABC,

$$\alpha + \theta + r + 90^0 = 180^0 \tag{5.3}$$

so $\theta = 90^0 - \alpha - r$ (5.4)

$$n_p \cos\theta = n_p \sin(\alpha + \theta) \tag{5.5}$$

From Snell's law at point B,

$$\sin i = n_p \sin r \tag{5.6}$$

$$r = \sin^{-1} \left(\frac{1}{n_p} \sin i\right) \tag{5.7}$$

Thus,

$$N = n_p \sin \left[a + \sin^{-1}\left(\frac{1}{n_p} \sin i\right)\right] \tag{5.8}$$

To measure the angle of incidence and the prism angle, a precision rotating table as shown in figure 5.1 is used. The angle measurement is carried out with a resolution of 6 arc seconds. The prism refractive index is measured to an accuracy of 4 decimal places using an Abbe' refractometer. For glass waveguides (substrate refractive index = 1.5125), a Schott glass (SF18) prism with n_p = 1.7167 (at λ = 0.6328 μm) is used. An output prism can be used to couple the guided energy out of the waveguide. To improve the sensitivity of the method, the beam is mechanically chopped at approximately 1 KHz and an output prism-detector combination is used in conjunction with a precision lock-in amplifier (Princeton Applied Research Model 124A) to detect the guided light amplitude. The point of maximum coupling is determined as the input incident angle is slowly increased by rotating the table, avoiding any backlash that may be present in the rotating table. This method greatly facilitates precise determination of incident angles where coupling occurs.

5.2 Propagation Loss Measurement

There are two types of losses which contribute to the propagation loss in optical waveguides: absorption losses and scattering losses.

The absorption losses are caused by the presence of impurities, especially the transition metal and hydroxyl ions (O-H). These losses are kept small by controlling the composition of the substrate glass. Ultra-clean processing environment is used while fabricating the substrate glass slides. The bulk glass manufacturers provide glasses (e.g., Schott S-8011) with transition metal impurities less than a few parts per million.

The scattering losses again are of two types. volume scattering and surface scattering. Volume scattering is caused by imperfections such as voids, crystalline defects, etc., within the volume of the waveguide. This type of loss depends very strongly on the relative size of the imperfections in comparison with the wavelength of light in the material. In most of the optical quality glasses, volume imperfections are small compared to the wavelength as well as few in number. As a result, the volume scattering loss is negligible compared to the surface scattering loss.

Surface scattering loss can be significant particularly for the fundamental mode in an asymmetrical graded-index waveguide because most of the guided energy in this case is confined to the region of higher refractive index which happens to be near the surface. The estimation of propagation loss is important in the waveguide design and fabrication because from an application point of view, the waveguide should have as low an insertion loss as possible and propagation loss is one component of the insertion loss.

To measure the propagation loss in planar surface waveguides, one could, in principle, use a two prism method in which a mode is excited by the input prism and the output power is measured by moving the output prism along the length of the waveguide. The plot of output power vs. distance has a negative slope as some power is either absorbed by the impurities or lost by scattering. The magnitude of the slope is the attenuation of the waveguide. To have a reliable measurement, however, it is necessary to keep the same coupling for each of the prisms at all positions of the output prism. This condition seems rather restrictive as input prism tends to get disturbed while moving the output prism. In addition, extreme care is needed to avoid spoiling of the guide surface at the contact point of the output prism.

An improved 3-prism method [Wo80] in which the results are independent of the prism coupling coefficients is used to measure the propagation loss. The measurement set-up is shown in figure 5.3.

Let P_a and P_b be the output powers of prisms A and B respectively. γ_A and γ_B are the coupling coefficients at the output prisms.

Then

$$P_a = \gamma_A\, P(z_1) \tag{5.9}$$

$$P_b = \gamma_B\, P(z_2) \tag{5.10}$$

where $P(z_i)$ = power travelling at point z_i.

Let α be the attenuation in the waveguide.

Then

$$P(z_2) = [P(z_1) - P_a]\, e^{-\alpha d} \tag{5.11}$$

so

$$P_b = \gamma_B[P(z_1 - \gamma_A\, P(z_1)]\, e^{-\alpha d} \tag{5.12}$$

Let $\gamma_a = 0$, i.e., Prism A is removed and the power output at Prism B be P_{b0}

$$P_{b0} = \gamma_B [P(z_1)]\ e^{-\alpha d} \qquad (5.13)$$

$$\Delta P_b = P_b - P_{b0} = \gamma_B \gamma_A\ P(z_1)\ e^{-\alpha d} \qquad (5.14)$$

$$\therefore \qquad \frac{P_a P_{b0}}{\Delta P_b} = P(z_1) \qquad (5.15)$$

From equation (5.15), it is seen that the expressions for $P(z_1)$, the power propagating at z_1, has no γ's in it. So $P(z_1)$ can be estimated without the knowledge of coupling coefficients γ_A and γ_B. Thus, by moving the Prism A, i.e., by changing z_1, one can find the power along the different points of the waveguide.

This method is used to measure the propagation loss of waveguides made on several substrates. Figure 5.4 shows the plots of relative power level vs. distance. The Labnate glass, which is an ordinary microscope slide glass, has a loss of approximately 1 dB/cm. A special batch of glass made by Schott Optical Glass Inc. shows a considerable reduction in loss (≈ 0.2 dB/cm) as the impurities in this glass are guaranteed to be less than about 10 parts per million.

5.3 Index Profile Measurement

Refractive index profile measurement techniques fall into the following two categories:

1. Optical interferometric technique: In this method, the index profile is determined by measuring the optical phase shift induced by the refractive index variation. The method uses a Mach-Zehnder or a similar type of interferometer to examine the polished slice of the waveguide. This technique is applicable essentially to relatively deeper waveguides (few tens of microns), which are generally multimode. For waveguides with effective depths in the range of 6-10 μm, cross-section preparation is somewhat difficult because of the chipping and the rounding of edges can occur place while polishing thin slices of the waveguides.

2. Surface analytical techniques: Surface analysis involves the determination of silver ion concentration profile by using one of the destructive surface analysis methods, e.g., X-ray microprobe, Auger spectroscopy, Secondary ion mass spectroscopy, etc. The implicit assumption in these methods is that the silver ion concentration profile matches the refractive index profile which is valid in the case of $Ag^+ - Na^+$ exchanged waveguides because the presence of silver ions is solely responsible for an increase in the refractive index and the concentration of silver ions is low.

Since this project deals with the fabrication and characterization of single mode glass waveguides whose depths are typically in the range of 6-8 μm, the optical interferometric techniques were not used for index profile determination. A Commercial Mach Zehnder interferometer is also not available. Several other groups working on glass waveguides have been using Electron Probe Micro Analysis (EPMA), frequently referred to as electron micro probe [St77, Li82]. The equipment needed for this technique is not available at the University of Florida. A new and simple method using scanning electron microscope (SEM) is developed for the index profile measurements.

In an SEM, the specimen is bombarded with an accelerated beam of electrons with the accelerating voltage in the range of 20-50 KV. The specimen generates two types of electrons, the secondary electrons and the backscattered electrons [Go81].

The secondary electrons are low energy electrons (less than 50 eV), generated primarily by inelastic scattering of the incident electron beam. Since the secondary electrons are generated with low kinetic energy, they usually come from the surface and carry information about the surface topography. Their yield is relatively insensitive to the composition of the specimen and it shows no strong trend with the atomic number of specimen.

The process of back scattering usually takes place as a result of a sequence of elastic scattering events in which the net change in the direction is sufficient to carry the incident electrons out of the specimen. The back scattered electrons are high energy electrons (greater than 100 eV) whose yield is defined by a parameter η, the backscattered electron coefficient, defined as

$$\eta = \frac{n_{BS}}{n_B} = \frac{i_{BS}}{i_B}$$

where

n_{BS} = number of backscattered electrons

n_B = number of beam electrons

i_{BS} = back scattered electron current

i_B = beam current.

If the backscattering coefficient η is measured as a function of the atomic number z, the relationship is given by

$$\eta = -0.0254 + 0.016z - 1.86 \times 10^{-4}z^2 + 8.3 \times 10^{7}z^3 \quad [5.16]$$

This relationship is plotted in figure 5.5.

When the target is a homogenous mixture of several elements, a simple rule of mixture based on the weight fraction of the components is found to apply

$$\eta_{\text{mixture}} = \sum \eta_i C_i \qquad (5.17)$$

where η_i is the backscattering coefficient for the pure element and C_i is the weight fraction of that element. Experimental measurements indicate that the backscattering coefficient does not depend upon the beam energy [Go81].

In the $Ag^+ - Na^+$ exchanged waveguides, the substrate material mainly contains ions, such as Na^+, Si^{4+}, O^{--}, Ca^{++}, etc. while the waveguiding region has additional silver ions (Ag^+). The atomic number of Ag (47) being higher than that of Na (12) and Si (14), the back-scattering coefficient of Ag is quite higher than that of Na and Si, as shown in figure 5.5. As a consequence of this, low concentration of silver ions in glass (which is true in the case of glass waveguides), still contributes significantly to the yield of the backscattered electrons. Thus, if the sample is polished across the edge of the waveguide and scanned in the SEM, the backscattered electron intensity profile gives a good approximation of the silver ion concentration profile and thus, of the index profile. The SEM is calibrated with high accuracy and can resolve spatial dimensions with high resolution, enabling this method to give accurate estimates of the index profile and the diffusion depth as well.

The procedure can be outlined as follows. The waveguide is polished in a plane perpendicular to the guiding direction. A thin layer of epoxy is applied to the surface of the waveguide and a glass slide made from the same bulk material (or a glass pad of similar hardness) is stuck to the surface before polishing. This prevents rounding or chipping at the edges of the waveguide while polishing. The polishing is done in two steps. Rough polishing with SiC powder and fine polishing with a 1 micron diamond paste. Glass, being a dielectric material, needs some conductive coating to drain the charge built up from the incident electron beam. A carbon coating (50 Å thick), has produced good results. Since the atomic number of carbon (6) is much lower than that of silver (47), the carbon coating does not interfere with the measurements. The sample is mounted on the SEM, and both the secondary electron and the backscattered signals are displayed simultaneously on the output screen split in two halves. In SEM terminology this display is called "Compo+Topo", Compo for composition and Topo for topography. Figure 5.6 illustrates such a "Compo + Topo" photograph. The left half of the picture is the secondary electron signal or "Topo". The absence of any pattern indicates that there is no surface roughness, confirming that the polishing is perfect. The right half of the picture is the display of the backscattered signal. The brightness is due to the presence of silver ions diffused in the glass. The slanted vertical line represents the epoxy layer. The epoxy being a high molecular weight organic compound, it contributes little to the yield of backscattering. A single line scan of the backscattering signal gives the index profile as shown in figure 5.7. The big dip in the signal corresponds to the epoxy layer. It serves as a good marker to locate the surface of the waveguide. Such a reference point is essential, especially while measuring the diffusion depth. The profile in figure 5.7 is of a waveguide fabricated by silver ion diffusion, without an applied electric field. It looks essentially like a complementary error function, giving an experimental confirmation of the results of diffusion simulation, as reported in Chapter Two. The profile is calibrated in the depth direction, i.e., a horizontal line represents a distance of 10 μm as shown in the photograph. Figure 5.8 shows the index profile resulting from a field assisted silver ion diffusion. The profile is essentially like a step, which again confirms the results of the numerical solutions of the differential equation 3.22. As seen in the figures 5.7 and 5.8, the waveguides with field assisted diffusion are considerably deeper (≃ 22 μm), than those made with ordinary diffusion (≃ 6 μm). This again confirms the results of diffusion simulation, as can be seen by comparing figures 3.2 and 3.3.

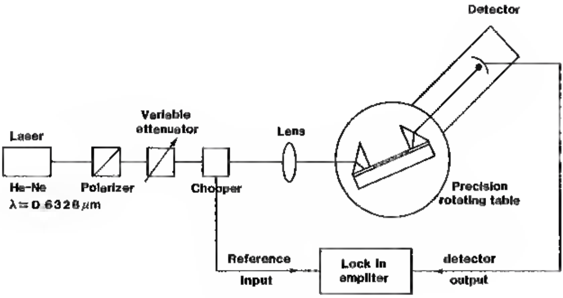
Laser
He-Ne
λ = 0.6328 μm
Polarizer
Variable attenuator
Chopper
Lens
Detector
Precision rotating table
Reference
input
Lock in amplifier
detector
output

Figure 5.1 Prism coupler set-up

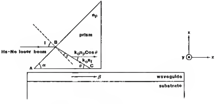
n_p
prism
I
B
He-Ne laser beam
$k_0 n_p \cos\theta$
r
$k_0 n_f$
A
α
θ
C
β
waveguide
substrate
x
y
z

Figure 5.2 Ray diagram for the prism coupler

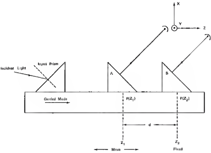
X
Y
Z
Incident Light
Input Prism
A
B
Guided Mode
$P(Z_1)$
$P(Z_2)$
d
Z_1
Z_2
Move
Fixed

Figure 5.3 Three prism method for loss measurement

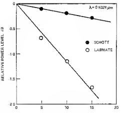

Figure 5.4 Loss measurement at 0.6328 micron

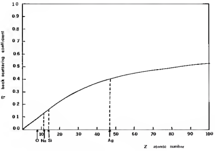

Figure 5.5 Backscattering coefficient as a function of the atomic number

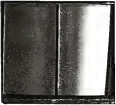

Figure 5.6 "Compo + Topo" photograph by the scanning electron microscope

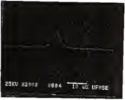
25KU X2000
0004
10.0U UFMSE

Figure 5.7 Index profile of a planar glass waveguide fabricated by diffusion without applied field

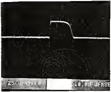

Figure 5.8 Index profile of a planar glass waveguide fabricated by diffusion with applied field

CHAPTER SIX
PLANAR WAVEGUIDE DESIGN PROCEDURE

6.1 Relations Between the Process and the Device Parameters

In this section, experimental results of the diffusion studies and modal behavior of planar glass waveguides is described. The planar glass waveguides fabricated by diffusion without an applied electric field have a complementary error function type index profile. The theoretical treatment presented in Chapter Three (figure 3.2) has been confirmed experimentally using SEM analysis in Chapter Five (figure 5.7). The b-V characteristics for this highly asymmetric profile have been determined by solving the normalized mode dispersion equation in Chapter Two (figure 2.9). A combination of these theoretical results and experimental investigation is used to find the links between the process and the device parameters. The experimental procedure is outlined below.

Several sets of single mode and multimode waveguides are fabricated using Labmate microscope slides for different values of the process parameters, C_o (Ag^+ concentration in bath) and t (diffusion time). For a particular batch, a known value of C_o is generated using the electrolytic technique described in Chapter Four, and waveguides are fabricated for times ranging from 20-120 minutes. Prism coupling technique described in Chapter Five is used to excite the modes and to estimate the mode indices (equation (5.8)). A computer program is written to estimate the diffusion constant D and the maximum index change Δn. The procedure is described as follows.

As before, the V parameter is defined as

$$V = \frac{2\pi}{\lambda}\, d\sqrt{2n_b\Delta n} \qquad (6.1)$$

where

λ = wavelength of operation

d = waveguide depth

n_b = builk refractive index

Δn = maximum change in the refractive index.

For complementary error function the wavguide depth d is given by

$$d = \sqrt{Dt} \qquad (6.2)$$

where

D = diffusion coefficient

t = time of diffusion.

Thus,

$$V = \frac{2\pi}{\lambda}\sqrt{2Dt}\cdot\sqrt{2n_b\Delta n} \qquad (6.3)$$

For mode index measurement a He-Ne laser is used for which $\lambda = 0.6328$ μm. The bulk refractive index n_b is measured up to four decimal places using an Abbe' refractometer. For Labmate glass, $n_b = 1.5125$. Thus, at $\lambda = 0.6328$ μm,

$$V = (2.442 \times 10^7)\sqrt{Dt\Delta n} \qquad (6.4)$$

Now the normalized mode index b for an asymmetrical graded index waveguide is defined as

$$b = \frac{N^2 - n_b^2}{n_s^2 - n_b^2} \qquad (6.5)$$

where

N = mode index

n_s = surface index = $n_b + \Delta n$.

For small index approximation (which is valid for glass waveguides), $\Delta n << n_b$ so that

$$b \approx \frac{N-n_b}{\Delta n} \tag{6.6}$$

From equations (6.4) and (6.6) it is seen that for a given glass substrate and a given wavelength of operation, b and V are functions of D, Δn and t. Δn depends upon C_o, the concentration of Ag^+ in bath. Thus, a set of waveguides fabricated with the same C_o but with different t have the same Δn but different depths, hence different V numbers. The computer program reads as its input data: mode orders, mode indices and diffusion times, for a set of waveguides with the same Δn. A min-max error algorithm is used for fitting experimental data into the theoretically derived b-V characteristics (figure 2.9). The values of D and Δn are initially assumed and for this choice, b and V are calculated from equations (6.4) and (6.6). The error is defined as the largest difference between the b's calculated from the theoretical characteristics and those calculated from the measured mode indices. The values of Δn and D are then varied over a prespecified range and the error calculations are repeated. The error contours for the points in the Δn-D plane are plotted as shown in figure 6.1. The contours show that the error has a minimum and the values of Δn and D corresponding to this minimum are the best estimates.

The waveguides are fabricated with several values of C_0, and Δn is estimated for each C_0. The relationship between Δn and C_0 is plotted as shown in figure 6.2. The curve in the region where the value of C_0 is small is essentially linear. For guides with small number of modes (1-6), the relationship between Δn and C_0 can be approximated as

$$\Delta n \simeq 26.5\ C_0 \qquad (6.7)$$

where C_0 is expressed as the mole fractions of silver ions in the bath.

This is an important link between the device parameter Δn and the process parameter C_0. This empirical relation is valid for Labmate slides that are used in our experiments. It needs to be redetermined if the weight fraction of Na_2O in the substrate material is changed. However, for the weight fraction in the neighborhood of 10-15%, an order of magnitude estimate established by equation (6.7) is valid.

To estimate the variation of the diffusion coefficient D with temperature T, three batches of waveguides are fabricated at 330, 354 and 364°C. The diffusion coefficient at these temperatures is estimated by the computer program mentioned above. The variation of D with T is given by an Arhenius type relation [Do64],

$$D(T) = D_o e^{-\Delta H/RT} \qquad (6.8)$$

where

ΔH = Activation Energy and

R = Gas Constant, 8.314 J/K°-mole.

Taking logarithm

$$\ell n\ D = \ell n D_o - (\Delta H)/RT \qquad (6.9)$$

Thus, the slope of the curve $\ell n\ D$ vs. $(1/T)$ gives the value of $\Delta H/R$. As shown in figure 6.3, ΔH is estmiated to be 8.933×10^4J. Also

$$D_o = 1.1906 \times 10^{-7}\ m^2/sec$$

Since for the glass waveguide fabrication, the diffusion time is of the order of tens of minutes and the diffusion depth is of the order of a few microns, D is expressed in micrometer²/minute. The temperature range is restricted as $NaNO_3$ melts at 307°C and decompose at 380°C [CR83]. Figure 6.4 shows the plot of D vs. T over the relevant temperature range. It is seen that the curve can be approximated by two linear segments with a transition around 353°C. Beyond 353°C, D changes rapidly with T so that in this region, the temperature fluctuations during fabrication will cause significant changes in D resulting in a large variation in the guide depth d. This indicates that the diffusion temperature should be chosen between 307°C and 353°C. During the experiments it is observed that a temperature gradient of as much as 20°C can exist in the bath and hence it is recommended to choose 330°C as the diffusion temperature, which is sufficiently higher than 307°C (the melting point of $NaNO_3$).

At 330°C, the diffusion coefficient has a value,

$$D = 0.129\ \mu m^2/\text{minute}$$

Substituting this value in equation (6.2),

$$d = 0.718 \sqrt{t} \tag{6.10}$$

This is the second important link between the device parameter d and the process parameter t.

6.2 Design Procedure

Using the relations 6.7 and 6.10, a systematic design procedure is formulated as described below [La84d].

The normalized dispersion equation for an asymmetrical, graded index planar waveguide is given by equation (2.11). At cut-off, $X_t' \to \infty$ and $b = 0$.

For complementary error function profile, $f(x') = \mathrm{erfc}(x')$.

Thus, V_{cm}, the value of V number at cut-off of the m^{th} mode is given by

$$V_{cm} \int_0^\infty \sqrt{\mathrm{erfc}(x')}\, dx' = \frac{(4m+3)\pi}{4} \qquad (6.11)$$

Since $\mathrm{erfc}(x')$ is a monotone decreasing function and $\mathrm{erfc}(2) = 0.0005$,

$$\int_0^\infty \sqrt{\mathrm{erfc}(x')}\, dx' \simeq \int_0^2 \sqrt{\mathrm{erfc}(x')}\, dx' \qquad (6.12)$$

The integral on the right hand side of equation (6.12) is evaluated numerically and its value is found to be 0.89. Thus,

$$(0.89)\ V_{cm} = \frac{(4m+3)\pi}{4} \qquad (6.13)$$

From equation (6.3), (6.7) and (6.10),

for $\lambda = .6328\ \mu m$, $n_b = 1.5125$ and $D = 0.129\ \mu m^2/min$,

$$V = 63.85 \sqrt{t\ C_o} \qquad (6.14)$$

from equations (6.13) and (6.14),

$$V_{cm} = \frac{(4m+3)\pi}{4\cdot(0.89)} = (63.85)\sqrt{t\ C_o}$$

Thus,

$$t\ C_o = (1.91 \times 10^{-4})(4m+3)^2 \qquad (6.15)$$

For various values of m, the relations between t and C_o as given by equation (6.15) are plotted in figure 6.5. Since these curves distinguish the regions of various modes, the design can be done entirely using the process parameters, making the device parameters invisible in the design procedure. For example, for a given time of diffusion (as decided by the required waveguide depth), one can find the value of C_o which keeps the waveguide single mode. Generation of this value of C_o can be done precisely using the electrolytic process described in Chapter Four. The inherent capability of this process to generate arbitrary values of C_o can be used together with these curves to fabricate waveguides supporting a specific number of modes. Since the variation of refractive index with wavelength (material dispersion) is rather small, the relation between Δn and C_o given by equation (6.7) is expected to be valid for other wavelengths too. Thus, similar design curves can be plotted for any other wavelength, e.g., for λ = 1.32 μm as shown in figure 6.6. The validity of the curves for λ = 0.6328 μm is experimentally confirmed by fabricating various graded index (erfc) waveguides by electrolytic release technique and evaluating them using the prism coupler.

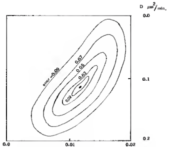

Figure 6.1 Error contours

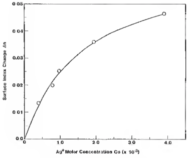

Figure 6.2 Δn − C_0 curve for Labmate glass

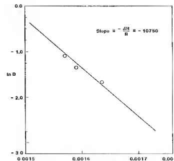

Figure 6.3 Estimation of ΔH for Labmate glass

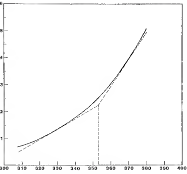

Figure 6.4 D - T curve for Labrate glass

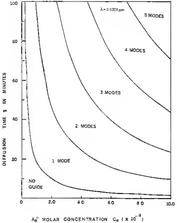

Figure 6.5 Design curves for λ=0.6328 micrometer

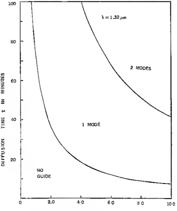

Figure 6.6 Design curves for $\lambda = 1.32$ micrometers

CHAPTER SEVEN
SCOPE FOR FUTURE WORK

In this chapter, the work partially completed in the course of this project is described, followed by a brief description of the research that is needed to complete the study of $Ag^+ - Na^+$ ion-exchanged waveguides.

7.1 Mode Profile Measurement

Mode profile is an important propagation parameter for both the surface and buried waveguides. When two waveguides are connected end to end for coupling, the efficiency of power transfer depends upon the overlap of the fields in these waveguides. Thus, in a variety of coupling problems such as laser to fiber, laser to waveguide, fiber to waveguide and waveguide to waveguide coupling, it is necessary to undertake an experimental determination of the mode profiles. Two methods are typically used to carry out the mode profile measurements. Both use an imaging lens of short focal length placed near the waveguide to magnify (250-500 X) the mode profile. For a detection-measurement system, one method used a vidicon camera placed at the image plane and an oscilloscope to view the video signal [Ko82], while the other employs a suitable semiconductor photodetector with a small aperture to scan the image plan manually [Ke79].

The latter technique has a disadvantage of being manual, hence slow. With a video camera-oscilloscope combination, the entire profile can be viewed continuously and the signal from several successive frames can be averaged to smooth out the electronic noise of the video camera tube. This technique is used to observe the mode profiles of planar surface waveguides. The experimental set-up is shown in figure 7.1. A planar waveguide propagating three modes is polished at the output and to avoid scattering and is excited using a prism coupler at the input end. The modes are individually excited and the output is focused onto a COHU 2810R video camera. A Tektronix 7854 oscilloscope with digital storage and waveform calculation capabilities is used to smooth the data by averaging successive frames. Figures 7.2 - 7.4 show the profiles for the first three modes. Since the waveguide is made with silver ion diffusion without drift field, it essentially has a complementary error function type index profile for which the fields are calculated numerically in Chapter Two. As seen in figure 2.11, for the higher order modes, the inner lobes of the field profile have higher peak amplitudes. This theoretical result is confirmed experimentally as seen in figures 7.3 and 7.4.

This video camera-oscilloscope combination can be used to determine the mode profiles of channel waveguides and to measure their effective modal widths. These data are essential in designing channel waveguides which have low coupling loss with single mode fibers.

7.2 Buried Waveguide Fabrication

A two step diffusion process has been used in glass to from buried waveguides [Ch80, Li82]. In this process, a surface waveguide is formed by a field assisted diffusion of silver ions in the first step. This is followed by another field assisted diffusion in pure $NaNO_3$. The buried waveguide is formed as sodium ions replace silver ions at the surface. The following four process parameters control the nature of the index profile.

t_1 : Time of diffusion in the first step ($NaNO_3$ with Ag^+)

E_1 : Field applied in the first step

t_2 : Time of diffusion in the second step (pure $NaNO_3$)

E_2 : Field applied in the second step.

In the existing process, field E_1 in the range of 60-100 V/mm is used. This results in a step-like waveguide (as shown in figure 5.8), which when buried, produces a waveguide with a skewed index profile (figure 7.5). It was found experimentally that if no field is applied in the first step, then the resulting buried waveguide has a symmetric, fiber-like index profile as shown in figure 7.6. This is the first time a fiber-like profile has been achieved in a planar substrate. Further studies are necessary to understand the diffusion process used for burying the waveguides.

7.3 Channel Waveguide Fabrication

For the fabrication of channel waveguides, the same electrolytic process is used for diffusion in which the silver ions are allowed to diffuse only through the windows formed in a metal mask. Photolithographic techniques, extensively used in microelectronics are adapted for window pattern fabrication. Some of the older techniques such as wet chemical etching which have poor resolution have been replaced by a superior lift-off technique which is illustrated in figure 7.7. Aluminum is used as a masking material, but other metals such as Titanium could also be used. Figure 7.8 shows the SEM picture of a pattern made by lift-off. The high quality of the pattern can be clearly seen from the straightness of the windows and the sharpness of the edges.

The yield of the process is extremely poor (1 out of 5) due to lack of extremely clean photolithographic facilities. It is also necessary to determine the optimum combination of the process parameters (photoresist spinning speed, photoresist spinning time, exposure time and development time) to improve the yield. The substrates must be thoroughly cleaned before the photoresist deposition and this cleanliness should be maintained throughout the processing. Any dirt or micron size dust particle causes poor bondage between the substrate and photoresist resulting into broken photoresist patterns.

7.4 Future Applications

The knowhow generated in this project can be utilized for the design and fabrication of useful devices. Since glass has low Fresnel loss compared to $LiNbO_3$, the best insertion loss figure of 1 db for 1.3 cm waveguide [Ra82] can be improved by fabricating high quality single mode channel waveguides on glass substrate. Integrated optical components such as directional couplers, star and access couplers, wavelength filters, etc. can be designed and fabricated after perfecting the techniques for channel waveguide fabrication and characterization.

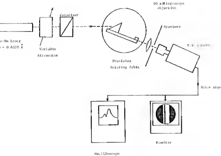
He-Ne Laser
λ = 0.6328 Å
Variable
Attenuator
Polarizer
40 x Microscope
objective
Aperture
Precision
Rotating Table
T.V. Camera
Video signal
Oscilloscope
Monitor

Figure 7.1 Set-up for measuring mode profiles in planar waveguides

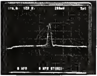

Figure 7.2 Mode profile for the fundamental mode

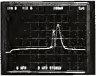

Figure 7.3   Mode profile for the first mode

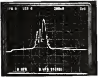

Figure 7.4 Mode profile for the second mode

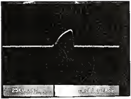

Figure 7.5 Skewed index profile of a buried waveguide

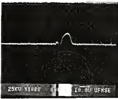

Figure 7.6 Symmetric, fiber-like index profile of a buried waveguide

PHOTOLITHOGRAPHIC LIFT-OFF TECHNIQUE

- Clean the substrate: Boil in TCE, acetone and methanol. Rinse in DI water. Stir dry with nitrogen. Hard bake for 60 minutes at 150° C
- Spin the photoresist: Use Shipley AZ 1450 J positive photoresist. Spin at 2500 RPM for 25 seconds. Softbake for 30 minutes at 95° C.
- UV exposure : Expose for 10 seconds.

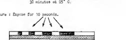

- Development: Mix Shipley 351 developer, 1 part in 6 parts DI water. Develop for 15-20 seconds. Rinse in DI water.

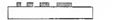

- Aluminum deposition: Deposit about 500-1000 angstorms of Al

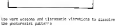

- Lift-off: Use warm acetone and ultrasonic vibrations to dissolve the photoresist patterns

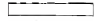

Figure 7.7 Photolithographic lift-off technique

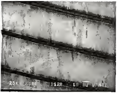

Figure 7.8 Aluminum mask pattern for channel waveguide fabrication

CHAPTER EIGHT
CONCLUSIONS

The aim of this project was to achieve a basic understanding of diffusion and optical wave propagation in glass and to use the results of this research to fabricate single mode waveguides with assured reproducibility. A combination of theoretical analysis, numerical simulation and experimental investigation is used to analyze silver ion diffusion and mode propagation in optical glass waveguides. Empirical relations linking the process and device parameters are derived and used subsequently to formulate a systematic procedure for designing single mode waveguides entirely in terms of the process parameters.

A list of significant results obtained in the course of this research work is given below:

1. Normalized propagation constants and mode profiles for arbitrary, highly asymmetrical graded index planar waveguides along with a closed form expression for the b-V characteristics for well-guided modes in buried waveguides.
2. Propagation analysis of channel waveguides with arbitrary index profiles and aspect ratios using a new

Variational-Finite difference method resulting in normalized solutions for the first time.

3. Diffusion simulation with and without applied electric field, for one dimensional and two dimensional diffusion of ionic species, e.g., Ag^+ ions (very low concentration) in a binary exchange scheme with Na^+ ions (high concentration) in glass.
4. Design of a novel electrolytic process for releasing silver ions in the molten $NaNO_3$ bath and development of a Galvanic cell transducer for in situ measurement of silver ion concentration.
5. Fabrication of planar single mode waveguides with very low propagation loss--0.2 db/cm and experimental confirmation of mode profiles in graded index planar waveguides.
6. Estimation of the diffusion coefficient and empirical derivation of Δn--C_0 curve for Labmate glass (Weight % of $Na_2O \simeq 10$-15%) and formulation of a systematic procedure for designing single mode planar waveguides.
7. Demonstration of a symmetric, buried waveguide with a fiber-like index profile, achieved using a two-step diffusion process.
8. Index profile measurement by a new and simple technique--scanning electron microscopy.

REFERENCES

[Al81] R. C. Alferness, "Guided wave devices for optical communication," IEEE J. Quantum Electron., QE-17, 946-959 (1981).

[Al78] R. C. Alferness and R. V. Schmidt, "Tunable optical waveguide directional coupler filter," Appl. Phys. Lett., 33, 161-162 (1978).

[Bl59] M. Blander, F. F. Blankenship and R. F. Newton, "The thermodynamics of dilute solutions of $AgNO_3$ and KCl in molten KNO_3, from electromotive force measurements, I. Experimental," J. Phy. Chem., 63, 1259-1261 (1959).

[Bo63] B. J. Boltaks, Diffusion in semiconductors, New York: Academic Press (1963).

[Ch80] G. Chartier, P. Collier, A. Guez, P. Jaussaud and Y. Won, "Graded indexed surface or buried waveguides by ion-exchange in glass," Appl. Opt., 19, 1092-1095 (1980).

[Co74] E. M. Conwell, "Modes in optical waveguides formed by diffusion," Appl. Phys. Lett., 23, 328-329 (1974).

[Cr56] J. Crank, Mathematics of diffusion, London: Oxford (1956).

[Cr83] CRC Handbook of Chemistry and Physics, Boca Raton: CRC Press (1983).

[Do64] R. H. Doremus, "Exchange and diffusion of ions in glass," J. Phy. Chem., 68, 2212-2218 (1964).

[Du61] F. R. Duke and H. M. Garfinkel, "Complex ions in fused salts. Cadmium and lead bromides," J. Phys. Chem., 65, 1627-1631 (1961).

[Fl56] S. N. Flengas and Sr E. Rideal, "On electrometric titration in fused salts," Proc. Roy. Soc. A., 233, 443-454 (1956).

[Fo60] G. Forsythe and W. R. Wasow, *Finite-difference methods for partial differential equations,* New York: John Wiley and Sons (1960).

[Gi80] T. G. Giallorenzi, "Optical communications research and technology. Fiber optics," Proc. IEEE, 66, 744-780 (1980).

[Gi73] T. G. Giallorenzi, E. J. West, R. Kirk, R. Ginther and R. A. Andrews, "Optical waveguides formed by thermal migration of ions in glass," Appl. Opt., 12, 1240-1245 (1973).

[Go69b] J. G. Goell, "A circular-harmonic computer analysis of rectangular dielectric waveguides," Bell Syst. Tech. J., 48, 2132-2160 (1969).

[Go69a] J. E. Goell and R. D. Standley, "Sputtered glass waveguides for integrated optics," Bell Syst. Tech. J., 48, 3445-3448 (1969).

[Go81] J. Goldstein, D. Newbury, P. Echlin, D. Joy, C. Fiory and E. Lifschin, *Scanning electron microscopy and X-ray microanalysis,* New York: Plenum Press (1981).

[He58] F. Helfferich and M. S. Plesset, "Ion exchange kinetics. A nonlinear diffusion problem," J. Chem. Phy., 28, 418-424 (1958).

[Ho75] G. B. Hocker and W. K. Burns, "Modes in diffused optical waveguides of arbitrary index profiles," IEEE J. Quantum Electron., QE-11, 270-276 (1975).

[Ho77] G. B. Hocker and W. K. Burns, "Mode dispersion in diffused channel waveguide by effective index method," Appl. Opt., 16, 113-118 (1977).

[Hu84] A. Huang, "Architectural considerations involved in the design of an optical digital compter," Proc. IEEE, 72, 780-786 (1984).

[In62] D. Inman, "A glass contained reference electrode for molten nitrate solvents," J. Sci. Instrum., 39, 391 (1962).

[Ir59] J. Irving and N. Mullineax, *Mathematics in physics and engineering,* New York: Academic Press (1959).

[Iz72] T. Izawa and S. Nakagome, "Optical waveguide formed by electrically induced migration of ions in glass plates," Appl. Phys. Lett., 21, 584-586 (1972).

[Ka73] I. P. Kaminow and J. R. Carruthers, "Optical waveguiding layers in LiNbO$_3$ and LiTaO$_3$s," Appl. Phys. Lett., 22, 326-328 (1973).

[Ke79] R. Keil and F. Auracher, "Coupling of single-mode Ti diffused LiNbO$_3$ waveguides to single mode fibers," Opt. Comm., 30, 23-28 (1979).

[Ko75] H. Kogelnik, "An introduction to integrated optics," IEEE Trans. Microwave Theory and Techniques, MTT-23, 2-16 (1975).

[Ko79] H. Kogelnik in "Integrated optics," edited by T. Tamir, Berlin: Springer-Verlag (1979), Chapter 2.

[Ko74] H. Kogelnik and V. Ramaswamy, "Scaling rules for thin film optical waveguides," Appl. Opt., 13, 1857-1862 (1974).

[Ko76] H. Kogelnik and R. V. Schmidt, "Switched directional couplers with alternating Δβ," IEEE J. Quantum Electron., QE-12, 396-401 (1976).

[Ko82] S. K. Korotky, W. J. Minford, L. L. Buhl, M. D. Divino and R. C. Alferness, "Mode size and method for estimating the propagation constant of single mode Ti:LiNbO$_3$ strip waveguides," IEEE J. Quantum Electron., QE-18, 1796-1801 (1982).

[La83] A. Lattes, H. Haus, F. Leonberger and E. Ippen, "An ultrafast all optical gate," IEEE J. Quantum Electron., QE-19, 1718-1723 (1983).

[La84c] R. K. Lagu, S. I. Najafi and V. Ramaswamy, "In situ measurement of ionic concentration during fabrication of ion-exchanged waveguides," Appl. Opt., 23, 3925-3930 (1984).

[La84a] R. K. Lagu and V. Ramaswamy, "A Variational Finite difference technique for analyzing channel waveguides with arbitrary index profiles and aspect ratios", to be submitted for publication to IEEE J. Lightwave Tech.

[La84b] R. K. Lagu and V. Ramaswamy, "Fabrication of single mode glass waveguides by electrolytic release of silver ions," Appl. Phys. Lett., 45, 117-118 (1984).

[La84d] R. K. Lagu and V. Ramaswamy, "A systematic procedure for the design and fabrication of single mode glass waveguides," to be submitted for publication to IEEE J. Lightwave Tech.

[Le82] F. J. Leonberger, C. E. Woodward and R. A. Becker, "4-bit 828 mega samples/s electro-optic guided wave analog-to-digital converter," Appl. Phys. Lett., 40, 565-568 (1982).

[Li82] H. J. Lilienhof, E. Voges, D. Ritter and P. Pantschew, "Field-induced index profiles of multimode ion-exchanged strip waveguides," IEEE J. Quantum Electron, QE-18, 1957-1962 (1982).

[Ma69] E. A. J. Marcatili, "Dielectric rectangular waveguides and directional couplers for integrated optics," Bell Syst. Tech. J., 48, 2071-2102 (1969).

[Ma73a] D. Marcuse, "TE modes of graded index slab waveguides," IEEE J. Quantum Electron , QE-9, 1000-1006 (1973).

[Ma73b] W. E. Martin, "Waveguide electrooptic modulation in II-VI compounds," J. Appl. Phys., 44, 3703-3707 (1973).

[Ma75] W. E. Martin, "A new waveguide switch/modulator for integrated optics," Appl. Phys. Lett., 26, 562-564 (1975).

[Ma73c] M. Matsuhara, "Analysis of TEM modes in dielectric waveguides by a variational method," J. Opt. Soc. Am., 63, 1514-1517 (1973).

[Mi73] S. E. Miller, E. A. Marcatili and T. Li, "Research toward optical fiber transmission systems, Part I: Transmission media," Proc. IEEE, 61, 1703-1726 (1973).

[Na84] S. I. Najafi, V. Ramaswamy and R. K. Lagu, "An improved method for fabricating ion-exchanged waveguides through electrolytic release of silver ions," Submitted for publication to IEEE J. Lightwave Technology (1984).

[Pi82] Ch. Pichot, "Exact numerical solution for the diffused channel waveguides," Opt. Comm., 41, 169-173 (1982).

[Ra82] V. Ramaswamy, R. C. Alferness and M. D. Divino, "High efficiency single mode fiber to Ti· LiNbO$ sub 3$ waveguide coupling," Electron Lett., 18, 30-31 (1982).

[Ra78] V. Ramaswamy, M. D. Divino and R. D. Standley, "Balanced bridge modulator switch using Ti-diffused $LiNbO_3$ strip waveguides," Appl. Phys. Lett., 32, 644-646 (1978).

[Ra83] V. Ramaswamy and R. K. Lagu, "Numerical field solution for an arbitrary asymmetrical graded-index planar waveguide," IEEE J. Lightwave Tech., LT-1, 408-417 (1983).

[Ra75] V. Ramaswamy and R. D. Standley, "Growth strains and losses in Nb diffused $LiTaO_3$ optical film waveguides," Appl. Phys. Lett., 26, 10-12 (1975).

[Ra73] V. Ramaswamy and H. P. Weber, "Low loss polymer films with adjustable refractive index," Appl. Opt., 12, 1581-1583 (1973).

[Sc68] E. R. Schineller, R. P. Flam and D. W. Wilmot, "Optical waveguides formed by proton irradiation of fused silica," J. Opt. Soc. Am., 58, 1171-1176 (1968).

[Sc74] R. V. Schmidt and I. P. Kaminow, "Metal diffused optical waveguides in $LiNbO_3$," Appl. Phys. Lett., 25, 258-260 (1974).

[Sm81] P. Smith and W. Tomlinson, "Bistable optical devices promise subpicosecond switching," IEEE Spectrum, 18, 26-33 (1981).

[Sm73] D. H. Smithgall and F. W. Dabby, "Graded index planar dielectric waveguides," IEEE J. Quantum Electron., QE-9, 1023-1028 (1973).

[St74] R. D. Standley and V. Ramaswamy, "Nb diffused $LiTaO_3$ optical waveguides--Planar and embedded strip waveguides," Appl. Phys. Lett., 25, 711-713 (1974).

[St77] G. Staward, C. A. Miller, P. J. R. Leybourn, C. D. W. Wilkinson and R. M. DeLarue, "Planar optical waveguides formed by silver ion migration in glass," IEEE J. Quantum Electron., QE-13, 192-202 (1977).

[Ta79b] A. Tai, I. Cindrish, J. Fienup and C. Aleksoff, "Optical residue arithmetic computer with programmable computation modules," Appl. Opt., 18, 2812-2823 (1979).

[Ta81] S. Tarucha, N. Minakata and J. Noda, "Complementary optical bistable switching and triode operation using $LiNbO_3$ directional couplers," IEEE J. Quantum Electron., QE-17, 321-324 (1981).

[Ta76] H. G. Taylor, "Dispersion characteristics of diffused channel waveguides," IEEE J. Quantum Electron., QE-12, 748-752 (1976).

[Ta79a] H. F. Taylor, "An optical analog-to-digital converter design and analysis," IEEE J. Quantum Electron., QE-15, 210-216 (1979).

[Ti71] P. K. Tien, "Light waves in thin films and integrated optics," Appl. Opt., 10, 1295-2413 (1971).

[Ul72] R. Ulrich and H. P. Weber, "Solution deposited thin films as passive and active light guides," Appl. Opt., 11, 428-434 (1972).

[Wo80] Y. H. Won, P. C. Jaussaud and G. H. Chartier, "Three prism loss measurement of optical waveguides," Appl. Phys. Lett., 37, 269-271 (1980).

[Ye75] C. Yeh, S. B. Dong and W. Oliver, "Arbitrarily shaped inhomogeneous optical fiber or integrated optical waveguides," J. Appl. Phys., 46, 2125-2129 (1975).

BIOGRAPHICAL SKETCH

Rajendra K. Lagu was born in Poona, India, on June 7, 1956. He received the B. Tech and M. Tech degrees in electrical engineering from the Indian Institute of Technology, Bombay, in May 1978 and December 1981 respectively. Since January 1982 he has been working towards his Ph.D. in electrical engineering at the University of Florida. He has been involved in research projects sponsored by Eglin Air Force Base and Air Force Office of Scientific Research. He is a member of Eta Kappa Nu, Tau Beta Pi, Phi Kappa Phi and the Institute of Electrical and Electronics Engineers (IEEE).

After graduation, he will be taking up a faculty position in the Department of Electrical and Computer Engineering, University of Iowa, Iowa City, Iowa.

I certify that I have read this study and that in my opinion it conforms to acceptable standards of scholarly presentation and is fully adequate, in scope and quality, as a dissertation for the degree of Doctor of Philosophy.

Ramu V. Ramaswamy, Chairman
Professor of Electrical Engineering

I certify that I have read this study and that in my opinion it conforms to acceptable standards of scholarly presentation and is fully adequate, in scope and quality, as a dissertation for the degree of Doctor of Philosophy.

Thomas E. Bullock

Thomas E. Bullock
Professor of Electrical Engineering

I certify that I have read this study and that in my opinion it conforms to acceptable standards of scholarly presentation and is fully adequate, in scope and quality, as a dissertation for the degree of Doctor of Philosophy.

Larry L. Hench
Professor of Materials Science and Engineering

I certify that I have read this study and that in my opinion it conforms to acceptable standards of scholarly presentation and is fully adequate, in scope and quality, as a dissertation for the degree of Doctor of Philosophy.

Charles E. Taylor
Professor of Engineering Sciences

I certify that I have read this study and that in my opinion it conforms to acceptable standards of scholarly presentation and is fully adequate, in scope and quality, as a dissertation for the degree of Doctor of Philosophy.

Martin A. Uman
Professor of Electrical Engineering

This dissertation was submitted to the Graduate Faculty of the College of Engineering and to the Graduate School, and was accepted as partial fulfillment of the requirements for the degree of Doctor of Philosophy.

May 1985

Hubert A Bevis

Dean, College of Engineering

Dean for Graduate Studies and Research